Natural Hazards
and Earth System
Sciences
Discussions

Seismogenic depth and seismic coupling estimation in the transition zone between Alps, Dinarides and Pannonian Basin for the new Slovenian seismic hazard model

Polona Zupančič[1], Barbara Šket Motnikar[1], Michele M. C. Carafa[3], Petra Jamšek Rupnik[2], Mladen Živčić[1], Vanja Kastelic[3], Gregor Rajh[1], Martina Čarman[1], Jure Atanackov[2], Andrej Gosar[1,4]

Correspondence to: Polona Zupančič (polona.zupancic@gov.si)

[1]Slovenian Environment Agency, Ljubljana, Slovenia
[2]Geological Survey of Slovenia, Ljubljana, Slovenia
[3]INGV
[4]University of Ljubljana, Faculty of Natural Sciences and Engineering, Ljubljana, Slovenia

Abstract. The seismogenic depth and seismic coupling are important inputs into seismic hazard estimates. Although the importance of seismic coupling is often overlooked, it significantly impacts seismic hazard results. We present an estimation of upper and lower seismogenic depth and hypocentral depth and seismic coupling in the transition zone between the Alps, Dinarides and Pannonian Basin, characterized by complex deformation pattern, highly variable crustal thickness, and moderate seismic hazard, supporting the development of the 2021 seismic hazard model of Slovenia. We estimated the lower seismogenic depth using seismological and geological data and compared them. The seismological estimate was based on two regional earthquake catalogues prepared for this study. In the area source model, estimates of lower seismogenic depth from seismological data are deeper or equal to the ones derived from geological data, except in one case. In the fault source model, we analyzed each fault individually and chose seismological lower depth estimates in 12 among 89 faults as more representative. The seismogenic thickness for each individual fault source was determined for seismic coupling determination. The seismic coupling was assessed by two approaches, i.e. we chose the most trusted value from the literature, and the value determined for each fault individually by using the approach based on the updated regional fault and earthquake datasets. The final estimate of seismic coupling ranges from 0.77 to 0.38. We compared the tectonic moment rate based on long-term slip rate using different values of seismic coupling with the seismic moment rate obtained from the earthquake catalogue. The analysis is done for the whole area, as well as for the individual area zones. The analysis of N-S components of estimated slip for the largest faults in the area of west Slovenia shows that the regional geologic and geodetic shortening rates are comparable. The total activity rate of three global seismic source models is compared, which gives up to a 10 % difference. Our results contribute to a better understanding of the seismic activity in the region and the approach for seismic coupling estimation can be applied in other similar regions.

Keywords: probabilistic seismic hazard assessment, parametrisation, seismic coupling, coupled thickness, seismogenic depth, Slovenia.

Natural Hazards
and Earth System
Sciences
Discussions

1. INTRODUCTION

Slovenia is located at the junction of the Alps, the Dinarides, and the Pannonian Basin, where different tectonic units contribute

35 to a complex deformation pattern (Schmid et al., 2020; Atanackov et al., 2021) (Fig. 1). Due to the Adria-Europe collision, the area is under N-S compression and experiences counterclockwise rotation, leading to activation of strike slip and reverse faulting in the area (e.g., Vrabec and Fodor, 2006; Placer et al., 2010; Poljak et al., 2010; Weber et al., 2010; Moulin et al., 2016; Atanackov et al., 2021; Grützner et al., 2021). The most recent damaging earthquakes occurred on the strike-slip Ravne Fault in 1998 and 2004 with m_w 5.6 and m_w 5.2, respectively (Bajc et al., 2001; Kastelic et al., 2008; Gosar et al., 2019a, 2019b).

40 Historical earthquakes with estimated moment magnitude m_w of up to 6.5 imply the region experiences moderate seismicity and has a moderate seismic hazard (Shedlock et al., 2000). Recently, the seismic hazard of the region has been assessed using a modern approach that takes into account knowledge of active faults and seismicity (Šket Motnikar et al., 2022; Atanackov et al., 2022). Understanding crustal structure is critical for developing a seismic hazard model, but available high-resolution data covering the whole studied area are sparse.

45 The crustal structure of the studied region was investigated by several authors either along profiles (e.g., Brückl et al., 2007), only with a few seismic stations (Michelini et al., 1998), or focused more on neighbouring (Najafabadi et al., 2022) or smaller regions (Bressan et al., 2009). Guidarelli et al. (2017) resolved the S-velocity structure of the crust and uppermost mantle and covered most of the territory of Slovenia and its surroundings. On the other hand, Kapuralić et al. (2019) computed a 3-D P-wave velocity model at the junction of the Dinarides and the Pannonian basin from local earthquake tomography (LET).

50 Neither of these inversions was able to resolve small-scale anomalies in the upper crust and inverted only for one type of velocity, which can bias either the velocity model or earthquake hypocentres. As we are using mainly seismological data in seismic hazard analysis and sometimes infer some parameters from geophysical data, this can affect the results. Recently, Rajh et al. (2022) inverted jointly for hypocentre parameters and 1-D P- and S-wave velocity models with station corrections. A joint inversion for 3-D P- and S-wave velocity models from LET (Rajh, 2022) improved the earthquake locations even further

55 and provided additional insight into the upper crustal structure. Both studies showed that the hypocentres located in previous studies were located too deep. Depth to the Mohorovičić discontinuity (Moho) in the studied area has been constrained by several different studies (e.g., Brückl et al., 2007; Grad et al., 2009; Stipčević et al., 2011; Guidarelli et al., 2017; Kapuralić et al., 2019; Stipčević et al., 2020). It ranges from about 38 to 45 km under the External Dinarides, becomes deeper towards the Alps, and shallows to about 30 and 25 km in the Adriatic foreland and the Pannonian Basin, respectively. Seismogenic depth

60 analysis for earthquakes in Slovenia (Rajh et al., 2017; Rajh and Gosar, 2018) identified at least two distinct areas with relatively shallow or deep earthquake foci. Upon close examination and as suggested already by several papers (Stipčević et al., 2020; Rajh et al., 2022), one can observe that the depth distribution of earthquakes approximately follows the varying Moho topography. This has an impact on the seismogenic depth of seismic sources.

65
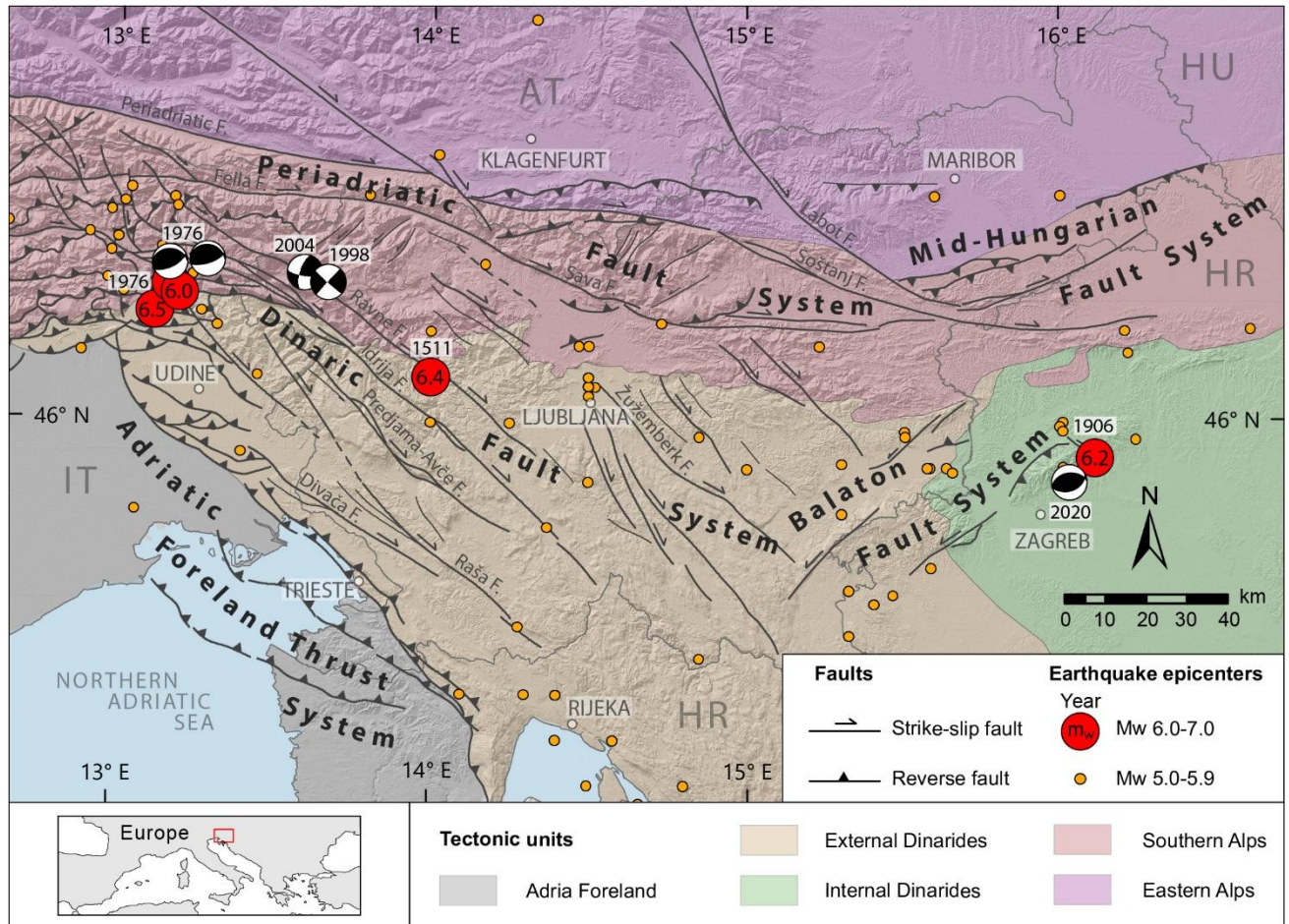
Figure 1. The seismotectonic setting of the study area: tectonic units are simplified from Schmid et al. (2020), active faults are summarized after Atanackov et al. (2021) and Poli and Zanferrari (2018), seismicity for $m_W > 5.0$ is from ARSO KPN2018 catalogue (1279-2018), focal mechanisms for $m_W > 5.0$ is from Bajc et al. (2001), Pondrelli et al. (2006), Kastelic (2008), and Herak et al. (2021).

In 2021, a new Slovenian seismic hazard model and map were developed (Šket Motnikar et al., 2022), as a result of a seven-year joint project of the Slovenian Environment Agency (ARSO) and the Geological Survey of Slovenia (GeoZS). The following year, the hazard map became part of Slovenian legislation for earthquake-resistant design. During the two-year transition period, in addition to the new Slovenian seismic hazard map, the previous hazard map from 2001 (ARSO, 2001; Lapajne et al., 2003) is still officially valid. We applied probabilistic seismic hazard assessment (PSHA), as introduced by Cornell (1968), which was later improved (e.g. Reiter, 1990; Baker et al., 2021). For the calculation of the new Slovenian seismic hazard map, the computer program OpenQuake was used (GEM, 2022).

In parallel to the development of the Slovenian hazard model, ESHM20 project, aiming to update the European seismic hazard model, was also underway (Danciu et al., 2021). This not only enabled us to exchange data and models, but we have also benefited from many discussions at regional meetings.

80

The new seismic hazard model includes three seismic source models (Fig. 2): a fault seismic source model (F), an area seismic source model (A), and a smoothed seismicity represented as a point seismic source model (P). The overview and results of the 2021 seismic hazard model for Slovenia, together with a description of the three seismic source models, their incorporation in seismic hazard calculation, and the estimation of most seismic source parameters are in detail explained in Šket Motnikar et

85   al. (2022). The parameterization tables for area seismic sources (AS) and fault seismic sources (FS), as well as shape files of their geometry, are provided in Pangaea online data portal (Atanackov et al., 2022).

One of the important features of the new PSHA, compared to the old one (Lapajne et al., 2003) is that for the first time in Slovenia, a thorough parameterization of active faults was performed and a related database was established (Atanackov et al.,

90   2021). The seismic activity of each fault source is defined by the slip rate parameter. Slip rates are usually estimated from all available data obtained with different methods covering very different time spans. Time spans range from several years (GNSS, PSInSAR, extensometer data), to several decades (leveling data), to thousands and tens of thousands of years (paleoseismic, geomorphic, geologic data) and even several million years (geologic data). Consequently, the slip rate data set is highly heterogeneous. As the tectonic moment rate is not released through earthquakes only, the slip realized through seismic activity

95   has to be estimated. A fraction of slip in the frictional regime that occurs during earthquakes is named seismic coupling (i.e. Bird and Kagan, 2004, Carafa et al., 2017) or seismic efficiency (Basili et al., 2023). In this paper, the term seismic coupling is used. There are not many studies on determining seismic coupling to be used in PSHA, especially on active shallow crust tectonic regions. The papers that deal with seismic coupling in the region (Ward, 1998; Burrato et al., 2008; Bus et al., 2009; Carafa et al., 2017) were studied and discussed in Sec. 2.4.

100

This study aims to estimate seismic coupling and seismogenic depth layers, which significantly impact the activity rate of fault seismogenic sources but were only briefly described in Šket Motnikar et al. (2022). The PSHA procedure (e.g., Baker et al., 2021) requires the estimation of upper and lower seismogenic depths for all types of seismic sources (e.g., fault, area, and point sources), and in addition, the expected hypocentral depth for AS and PS should be provided. Also, the seismogenic thickness

105   (difference between lower and upper seismogenic depth) is needed for estimating the seismic part of the slip rate (Bird and Kagan, 2004; Carafa et al., 2017). For the new Slovenian seismic hazard model, most of the parameters of the fault seismic source model are based only on the knowledge of active tectonic structures (Atanackov et al., 2021, 2022), since we kept the parameter estimation independent and uninfluenced by seismological data. On the other hand, the parameters for area source zones were mainly based on seismological data. Therefore, the seismogenic depth was determined using both geological and

110   seismological approaches.

In the continuation, we first present in detail the relevant data and methods for geological and seismological estimation of seismogenic depth. Besides the available seismic coupling values from the literature, we adopted the method developed by Carafa et al. (2017). In the second part, we discuss the obtained results of upper and lower seismogenic depth and hypocentral

115 depth. Applying the obtained seismic coupling, we compared the total seismicity as estimated from seismological and geological data. The comparison was made in terms of annual activity rate and seismic moment rates, both for the entire observation area and individual area source zones.

2. DATA AND METHODS

The first step in PSHA is a determination of the seismic source characterization (SSC) model that defines the spatial location
120 of future earthquakes, and their frequency and magnitude distribution. Seismic source characterization consists of developing a model that includes the historical earthquake catalogue, instrumental earthquake catalogue, and the development of a regional seismotectonic model. A key aspect of any SSC model building process is to consider all relevant and up-to-date seismotectonic, geological, and seismological data, models, and methods.

2.1. Seismic source characterization models

The geological, geophysical, geotechnical, and seismological data are the basis for the development of the regional seismotectonic model (Fig. 1). Paleoseismic, geomorphic, and geological data are of special importance to PSHA because they provide information about the seismic activity associated with long recurrence intervals, that is not captured with earthquake
130 catalogues and geodetic data (Morell et al., 2020).

The active faults map and the corresponding database, compiled by Atanackov et al. (2021), cover the territory of Slovenia and include cross-border faults and faults in the near vicinity. Besides the earthquake catalogues, they represent the main data for the parametrisation of fault and area seismic sources (Fig. 2). The F source model includes all known active faults that are
135 able to generate an earthquake of m_w 5.5 or higher. Each fault source is also given the probability of its activity in four categories (active 1.0, probable 0.7, potential 0.5, or questionable faults 0.25). The F source model consists of 89 fault seismic sources; 67 sources are parametrized by Atanackov et al. (2022), and the parameters for the remaining 22 fault sources were taken from the European Database of Seismogenic Faults (EDSF) (Basili et al., 2013).

140 Area source zones are the most standard type of seismic sources in PSHA. The A source model consists of 18 area source zones (Fig. 2) and covers the whole influential area (Šket Motnikar et al., 2022).
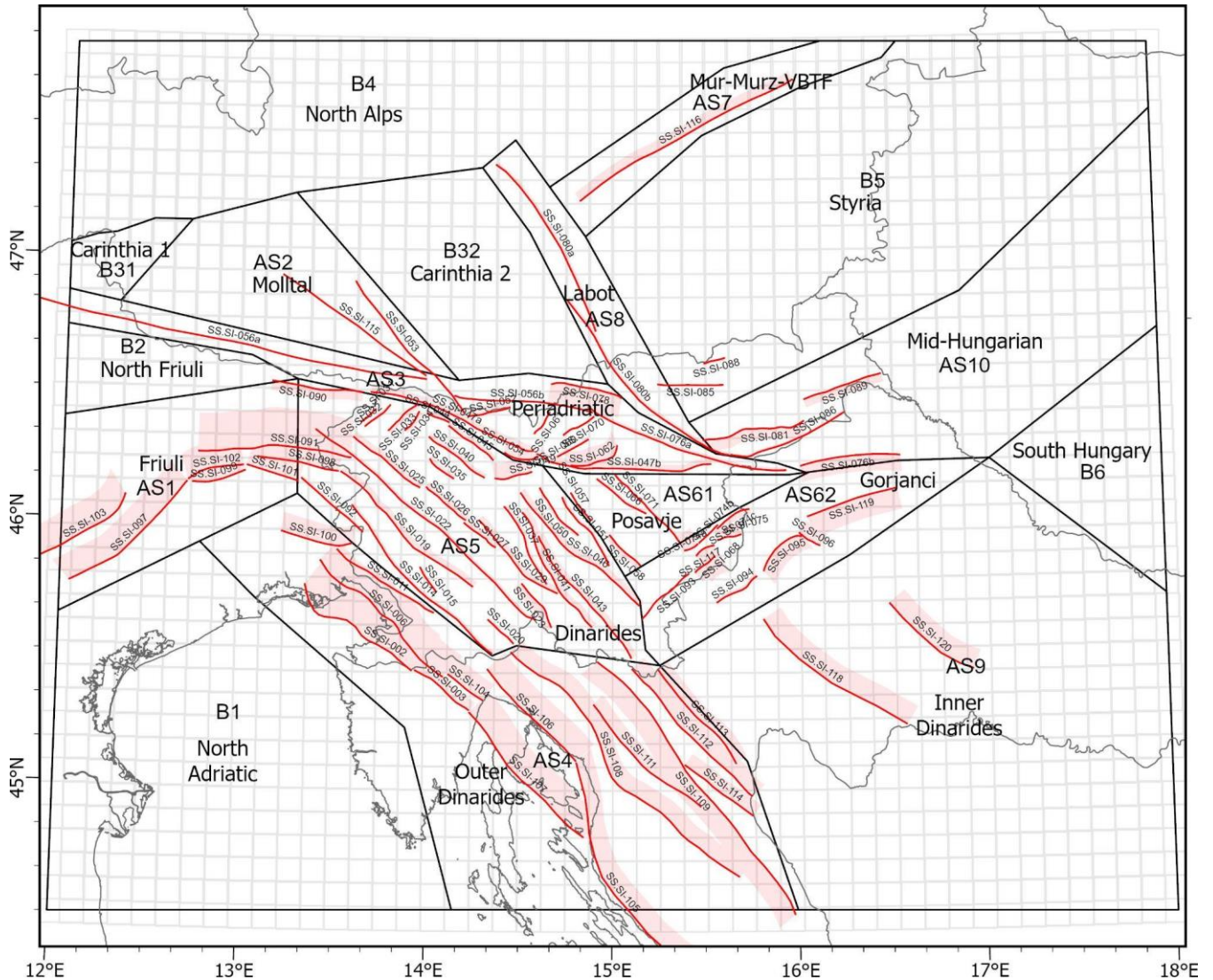
Figure 2: Seismic source characterization models: fault seismic sources with the surface projection of fault plane (red colour), area seismic sources (black polygons) and point seismic sources (grey rectangular grid).

2.2. Earthquake catalogues

The seismological information is based on two earthquake catalogues that were compiled for the new PSHA of Slovenia. The historical catalogue of larger earthquakes for Slovenia and the surrounding region (KPN2018) has a target completeness of m_w=3.5 (Šket Motnikar et al., 2022). There are 2867 earthquakes in the study area (12°E to 18°E and 44.5°N to 47.8°N). For the purpose of depth determination, the H_KPN18 catalogue was prepared, where only earthquakes from 1900 on were selected and earthquakes with unknown or zero depth were removed. There are 1477 earthquakes remaining for depth analysis in the H_KPN18 catalogue (black circles in Fig. 3).
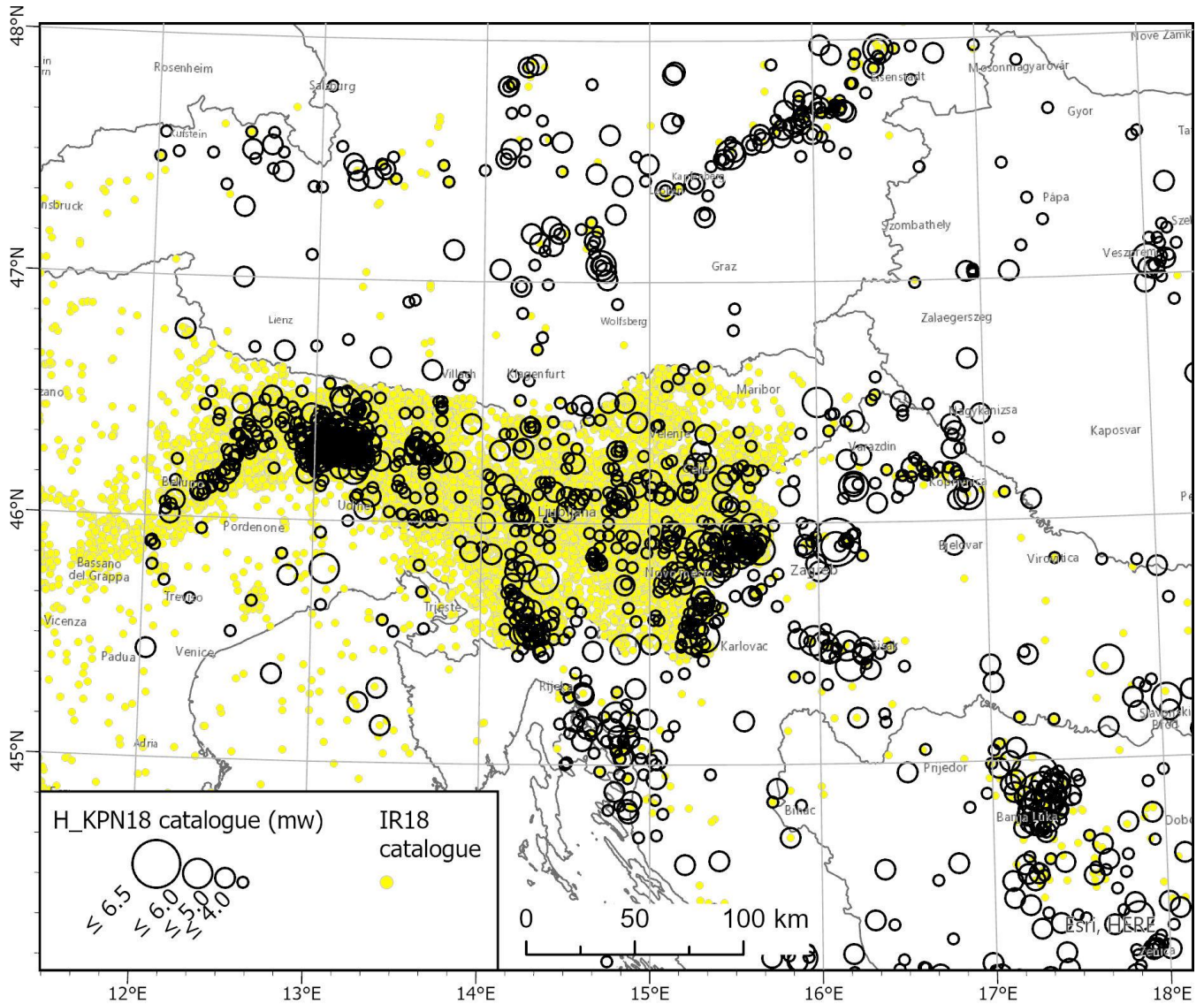
Figure 3: Earthquakes from H_KPN18 (black circles) and IR18 (yellow dots) catalogues used for depth determination of fault and area seismogenic sources.

155

In general, reliable hypocentre information can only be derived from earthquakes recorded with modern instruments. For the
160 territory of Slovenia, we have used the earthquake catalogue of instrumentally recorded earthquakes in the period 2004 – 2018
(ARSO, 2018). To cover the whole study area of interest we have also used the seismic catalogues of neighbouring countries:

7

the Friuli catalogue (INOGS, 1977-2014) from 1980 on, the Austrian catalogue (ZAMG, 2002; 1998-2014) from 1990 on and BSHAP catalogue (BSHAP-2, 2015) from 1990 on. From catalogues for the neighbouring countries, we removed the earthquakes with unknown or zero depth. From the Slovenian catalogue, we removed the earthquakes with unknown depth or

165 depth zero km, and poorly constrained earthquakes where the maximum azimuthal station gap is greater than 180 degrees and where the number of recording stations is smaller than 5. The 29018 earthquakes from all these catalogues were joined to the IR18 catalogue (yellow dots in Fig. 3).

The H_KPN18 and IR18 catalogues were used for seismogenic depth estimation, and consequently for seismic coupling

170 estimation. The declustered catalogue KPN2018 was used for seismic moment rate calculation.

2.3. Seismogenic depth

Seismic source (e.g. fault, area, or point source) represents the source that could produce seismicity. Therefore the seismogenic part of the lithosphere has to be constrained in depth. The upper and lower limits are called upper and lower seismogenic depth and can be assessed either based on knowledge of active tectonic structures or by studying the depth distribution of past

175 earthquakes. To take into account the uncertainty of earthquake depth determination, a chosen percentile depth cut-off was used. The seismogenic thickness (difference between lower and upper seismogenic depth) is also needed for the estimation of the seismic part of the slip rate.

The lower seismogenic depth was determined based on geological and seismological approaches. In Sec. 3, for each FS

180 individually, we decided which among the two (geological vs. seismological) lower seismogenic depth estimates is used for assessing the seismic part of the slip rate. For AS, the comparison between seismological and geological lower seismogenic depth showed that seismological estimates are deeper at all AS except for one source zone. For each AS, the deeper estimate is chosen for the final lower seismogenic depth.

185 The upper seismogenic depth is estimated geologically for all FS and AS. Additionally, the expected hypocentral depth should be given for AS and PS. It was estimated from measures of central tendency using seismological data.

All depths in earthquake catalogues and all assessed depths of seismogenic sources refer to the WGS 84 reference ellipsoid.

2.3.1. Geological depth estimation

190 The upper seismogenic depth for FS is estimated from known geological (based on published data, fieldwork, and geomorphologic analyses) and geophysical data interpretation. We assume that all faults that exhibit clear surface traces can produce a surface rupture in the event of large earthquakes. For the buried faults we consider the depth to the subsurface fault

tip as visible in the geophysical profiles. For some faults outside Slovenia (Friuli), the upper depth is taken from the literature
(Basili et al., 2013).

195

The upper seismogenic depth for AS is determined from geological information because there is no seismological information
to support any other value. The upper seismogenic depth value for all AS is 0 km because the majority of fault sources exhibit
surface traces and we assume that they can produce surface rupture in case of a large earthquake.

200   The upper seismogenic depth is therefore hypothetically set to 0 km both for FS and AS, except for known blind faults in the
FS model. This is based on the assumption that the fault zones mapped at the surface were formed by surface rupturing
earthquakes. However, exhumation processes bring on the surface also fault zones from previous tectonic phases that are
currently inactive, so our assumption includes uncertainties, mainly related to the unknown relationship between the surface
expression of faults and the underlying seismogenic structures. On the other hand, structurally immature faults may not have
205   easily recognizable fault traces at the surface, and in such a case, the FS has not been identified. The 0 km upper seismogenic
depth can be considered confirmed for the faults that were recognized as active with one of the surface investigation methods
(geomorphological offsets, outcrop observations, or shallow geophysics), testifying the surface rupturing paleoearthquakes.

The geological lower seismogenic depth estimation of the FS and AS is a comprehensive analysis incorporating various lines
210   of evidence, including published tectonic models, structural-geological and geophysical data, as well as the reinterpretation of
these data sets in the light of derived seismic source models. One important factor considered in this estimation is the presence
of detachments and their potential implications for seismic activity. Additionally, the intersection of the fault plane with other
fault planes within the model and constraints on fault geometry inferred from seismicity distribution are taken into account. It
is worth noting that the lower seismogenic depth of the nearest FS was adopted in the absence of any other data or argument.
215   This approach ensures a conservative estimate and serves as a reasonable starting point, considering the limited available
information. However, it is important to recognize the inherent uncertainties associated with this approach and acknowledge
the need for further investigations and data acquisition to refine the geological depth estimation in the future.

2.3.2. Seismological depth estimation

Seismological depth in the observed area was analyzed for various cell sizes and seismic source models (5×5 km^2 cells, 7.5×7.5
220   km^2 cells, 10×10 km^2 cells, AS, FS buffers). For each of them and both catalogues (IR18 and H_KPN18) minimum, maximum,
median, average, 90th, and 95th percentile of depth were calculated. To achieve robust depth estimates that are insensitive to
outliers (occasional earthquake locations at large depths), a 95th percentile depth cut-off was applied.

The IR18 catalogue shows an uneven distribution of earthquakes either because of spatially heterogeneous earthquake activity
225   rates or because of different catalogue's origins (different threshold magnitude/intensity, seismic network density). The best

Natural Hazards
and Earth System
Sciences
Discussions

Open Access

EGU

covered areas are Slovenia and Friuli, therefore, depth evaluation in these two areas is better than in other areas. We are aware of the problem that instrumentally recorded catalogues include mainly weak and moderate size earthquakes and that the large size earthquakes might not follow the same depth distribution. Therefore we also used the catalogue H_KPN18 with historical earthquakes to derive the second set of lower seismogenic depth estimates.

230

Based on this analysis, the seismological estimate of lower seismogenic depth in a given AS is chosen to be the deeper of the two 95th percentile (from IR18 and H_KPN18 catalogues) values. The exception is made where there is a large difference between the 95th and 90th percentile due to the small number of earthquakes. In such cases, the value of 95th percentile is strongly influenced by the few deepest earthquakes, for which the depth estimates are poorly constrained. In such cases, the

235   90th percentile of depth was chosen. If case of a single or no earthquakes inside the area source zone, the values for lower seismogenic depth from the neighbouring zone were adopted.

For seismological depth estimates of FS, we assessed the depth distribution of earthquakes with the IR18 catalogue only. For this purpose, the earthquake was attributed to the FS if it is less than 5 km from the surface projection of the FS plane (FS

240   buffer).

The values of the 50th percentile from IR18 and H_KPN18 don't differ much, but the H_KPN18 contains also strong earthquakes, therefore the expected hypocentral depth was determined as the 50th percentile (median) from the H_KPN18 catalogue. In case of a single or no earthquake inside the area source zone, the values for expected hypocentral depth from the

245   neighbouring zone were adopted.

2.4. Slip rate and seismic coupling

The seismic activity of each fault source in the F model is characterized by two key components: the slip rate parameter and its associated seismic component. In this study, we have undertaken a comprehensive estimation of slip rates by utilizing a

250   diverse range of data obtained from various projects, each employing distinct methodologies and objectives. The data collection spans significantly different time scales, enabling a robust analysis. The time spans encompassed in our investigation vary from short-term observations of a few years, including data obtained from GNSS (Global Navigation Satellite System), PSInSAR (Persistent Scatterer Interferometric Synthetic Aperture Radar), and extensometer measurements, to medium-term observations spanning several decades, derived from levelling data. Additionally, we incorporated long-term datasets covering

255   timeframes of thousands and tens of thousands of years, acquired through paleoseismic, geomorphological, and geological investigations, data spanning several million years, sourced from geological records. Consequently, the slip rate data set is highly heterogeneous (Atanackov et al., 2021, 2022). For each individual FS, we provided the minimum, maximum, and best

Natural Hazards
and Earth System
Sciences
Discussions
EGU
Open Access

estimate. It should be noted that the slip rates in the database of the Slovenian seismic source model (Atanackov et al., 2021, 2022) correspond to the total (seismic and aseismic) slip.

260

The seismic coupling c is defined as the fraction of slip in the frictional regime that occurs in earthquakes (e.g. Bird and Kagan, 2004, Carafa et al., 2017). We used two approaches for the determination of seismic coupling. In the first approach, we reviewed the existing literature and adopted the best assessment for the area under consideration. In the second approach, we determined the seismic coupling individually for each FS following Carafa et al. (2017). The values thus obtained were
265 compared in terms of seismic moments.

The seismic moment of a given fault source is defined as the product of the shear modulus of the crust μ, the area of the fault A, and the displacement D (Aki, 1966):

270 $M_{total} = \mu A D$,
$\qquad\qquad\qquad\qquad\qquad\qquad\qquad\qquad\qquad\qquad\qquad$ (1)

The total moment rate $\dot{M}_{total}$ is the average seismic moment of the selected fault source in the given time period:

$\dot{M}_{total} = \mu A S$,
$\qquad\qquad\qquad\qquad\qquad\qquad\qquad\qquad\qquad\qquad\qquad$ (2)

275

where S is the average slip rate.

Seismic moment M released through an earthquake can also be determined from the earthquake size and is calculated from its moment magnitude m_w using the Eq. (1) in (Kagan, 2002):

280

$M = 10^{1.5(m_w+6)}$.
$\qquad\qquad\qquad\qquad\qquad\qquad\qquad\qquad\qquad\qquad\qquad$ (3)

For the seismological calculation of seismic moment rate (denoted as $\dot{M}_{seis}$) based on the earthquake catalogue, we followed Eq. (7) in Kagan (2002):

285

$\dot{M}_{seis} = \frac{\alpha_0 m_t^\beta \Gamma(2-\beta)}{1-\beta} M_c^{1-\beta} exp(\frac{M_t}{M_c})$,
$\qquad\qquad\qquad\qquad\qquad\qquad\qquad\qquad$ (4)

where M_t is the threshold moment for the completeness of the catalogue, α_0 the total annual number of earthquakes above completeness magnitude m_t, M_c the corner (maximum) moment and β being the slope of the moment-frequency relation.

290 The tectonic moment rate (denoted as $\dot{M}_{tect}$), obtained from the geological data, was calculated with Eq. (5). Since not all of the fault energy is released through seismic events, the coupling parameter c is added to the equation,

$$\dot{M}_{tect} = c\dot{M}_{total} = c\mu AS .$$ (5)

295 The F source model consists of 89 FS, among which 67 sources are parametrized by Atanackov et al. (2022), and the remaining 22 FS were taken from the European Database of Seismogenic Faults (EDSF) (Basili et al., 2013). The slip rate values in the EDSF database already correspond to the seismically coupled part and were used as such for ESHM20 (Danciu et al., 2021). Therefore, in the case of these 22 FS, in this study, we used the slip rate data as they are, without any correction of seismic coupling (c=1).

300 Several authors have extensively investigated seismic coupling in the region, including Ward (1998), Burrato et al. (2008), Bus et al. (2009), and Carafa et al. (2017). These studies employ different methodologies, resulting in diverse outcomes regarding seismic coupling. Table 1 provides a summary of select papers.

The variable estimates of seismic coupling can be attributed to several factors. Firstly, the presence of different tectonic regions within the study area may introduce variations in seismic coupling behaviour. Secondly, the seismic catalogue used in these

305 studies may suffer from incompleteness, particularly in capturing infrequent large events with long return periods. Additionally, limited observational periods of GNSS data collection may also contribute to uncertainties in estimating seismic coupling. Finally, the combination of all the aforementioned factors could collectively contribute to the observed variability in seismic coupling estimates.

310 **Table 1: The seismic coupling as interpreted from the most appropriate literature.**

Author	Paper title	Considered area	Seismic coupling c (%)
Ward (1998)	On the consistency of earthquake moment rates and space geodetic strain rates: Europe	Italy Balkan world/Mediterranean	71 59 50
Bus et al. (2009)	Active crustal deformation in two seismogenic zones of the Pannonian region – GPS versus seismological observations	Central Pannonia Mur – Murz zone	17 34 - 58

2.4.1. Seismic coupling and coupling thickness of the seismogenic lithosphere

Carafa et al. (2017) proposed a method, which enables estimation of the seismic coupling individually for each fault seismic

315 source. The value depends on the coupled thickness of the seismogenic lithosphere (cz) which is defined as the product of the

difference between the upper and lower seismogenic depth (seismogenic thickness z) of the given fault source and its seismic coupling (c) for different fault kinematics (Table 2).

Table 2: The coupled thickness of seismogenic lithosphere (cz) for different fault kinematics according to Carafa et al., 2017.

	compressional faults	extensional faults	strike-slip faults
coupled thickness (cz) (km)	3.7 ± 0.7	$7.2^{+2.5}_{-1.5}$	4.8 ± 0.9

320

Considering the proposed method and values in Table 2, we estimated the seismic coupling c for each of the 67 FS.

For the calculation of the coupled thickness, we slightly corrected the estimation of the lower seismogenic depth for a few chosen FS (see Sec. 3). For the lower seismogenic depth, we used either the value from geological data (e.g. from the F model), applied for most FS, or the value determined from seismological data (e.g. from the A model). The criteria for choosing one or another value are described in the Sec. 3. The upper seismogenic depth was taken as estimated in the F model.

3. RESULTS AND DISCUSSION

3.1. Seismogenic depth

3.1.1. Fault source model

The lower seismogenic depth was estimated based on geological and seismological data. To decide, which of the two values better determines the coupled thickness, we compared the geologically determined lower depth with the histogram that presents the spatial distribution of the earthquakes' depth from the IR18 catalogue in the FS buffer. Also, the 5th and 95th percentile of depth are shown (Fig. 4). We have evaluated each FS separately using expert knowledge and several criteria.

For most of the FS, we chose the geological depth estimates. The most typical argumentations and examples (Fig. 4) are explained as follows. If the earthquakes contained in the FS buffer are deeper than the geological depth estimate:

- these earthquakes were either believed to belong to other neighbouring FS that are overlapping with the assessing source (SS.SI-049 in Fig. 4), or
- the knowledge of active tectonic structures is poor and we are not able to attribute these earthquakes to any of FS (SS.SI-20 in Fig. 4), or
- the FS due to its limited length cannot accommodate deeper earthquakes in order to respect the fault geometric aspect ratio of the tectonic structure (SS.SI-035 in Fig. 4).

In some cases, the earthquakes originate on the margins of the tectonic structure and are not representative of this structure (SS.SI-40 in Fig. 4). If the seismicity in the FS buffer is not as deep as the geological depth estimate and the FS is prominent (regional) – we believe that the too short time span of seismological observations and mainly weak events in the IR18 catalogue

Natural Hazards
and Earth System
Sciences
Open Access

EGU

Discussions

345   are not representative of the lower seismogenic depth of the structure (SS.SI.046 on Fig. 4). The geological depth estimates
       were also chosen for those FS where either geological depth estimates and earthquakes depth distribution match well (SS.SI-
       074a on Fig. 4) or earthquakes contained in the FS buffer are too few to reliably estimate the depth. The data published in
       EDSF (Basili et al., 2013) for the FS in the Friuli area are used as given in the database.

350   The seismologically determined lower seismogenic depth is a better choice for 12 FS because it can be assumed that the
       earthquakes are representing the behaviour of these structures better. This is true for the seismicity of prominent (also regional)
       structures where the earthquakes are considerably deeper than the geological depth estimates (SS.SI-019 in Fig. 4). Also the
       FS, for which the histograms show normal distribution, and the geological depth estimate is approximately at its median, we
       infer that the seismological data represent the behaviour of the structure better (SS.SI-032 on Fig. 4). The seismogenic lower
355   depth ranges from 5 km (SS.SI078 Northern Karavanke thrust fault) to 20 km (SS.SI-056a,b Sava W and E faults).

       Geological and seismological values of upper and lower seismogenic depth for all FS in the F model are available in Pangaea
       online portal, columns *Min depth_geo, Max depth_geo, Max depth_seismo* (Atanackov et al., 2022).

Natural Hazards
and Earth System
Sciences
Open Access
Discussions
EGU
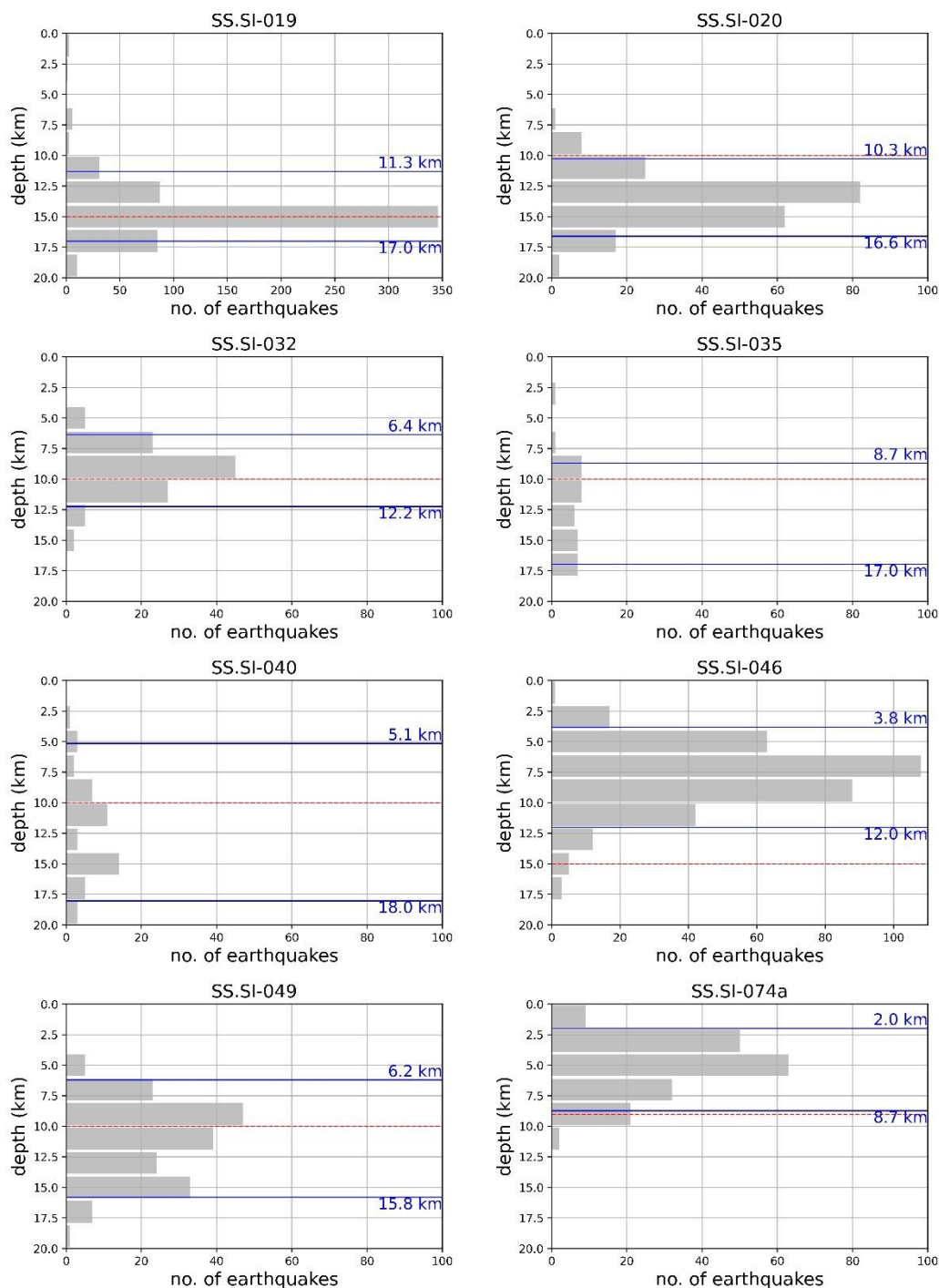
Figure 4: Some examples of IR18 catalogue earthquakes depth distribution within FS. Blue lines represent the 5th and 95th percentile respectively, and the red line denotes lower seismogenic depth based on knowledge of active tectonic structures.

15

3.1.2. Area source model

365   The spatial distribution of the 95th percentile of depth from IR18 catalogue earthquakes in 5x5 km^2 cells (Fig. 5) shows a good correlation of earthquake epicentres with depth to Moho (e.g., Brückl et al., 2007; Grad et al., 2009; Stipčević et al., 2020). Deeper hypocentres in the northwest, west and central regions generally correspond to more profound Moho levels. However, some shallow earthquakes (Bajc et al., 2001; Zupančič et al., 2001) in the Julian Alps, the area of the deepest regional Moho, show discordance between the general hypocentre-Moho depth relation, pointing to the importance of dedicated local studies

370   and also a better knowledge of local active fault characteristics. The epicentres originating in the eastern part of Slovenia around Posavje, Krško Basin and Gorjanci Mountains are the shallowest in the areas where Moho decreases. Catalogue IR18 includes mainly weak and moderate size earthquakes, thus the depth distribution of large size earthquakes might show a different distribution. The spatial distribution of depth from historic earthquakes (H_KPN18 catalogue) in 5x5 km^2 cells is not representative due to a small number of earthquakes in individual cells.

375   The estimates of the lower seismogenic depth for AS using catalogue IR18 are shown in Table 3 and Fig. 5 and 6, while the results in Table 4 correspond to the catalogue H_KPN18. The final value of the lower seismogenic depth represents the deeper among the geological and seismological estimates. For all AS but one (AS8 Labot), the seismological estimate is taken. The final values of lower seismogenic depth are mainly influenced by the historical earthquakes from the H_KPN18 catalogue and only partially reflect the depth pattern described above. The values of upper and lower seismogenic depths, and of hypocentral

380   depths are given in Table 5 and are shown in Fig. 7.

Table 3: Earthquake depth statistics per area source zone with IR18 catalogue (min, max, average, standard deviation, 50th, 90th, 95th percentile are in [km]).

Area source	No. of earthquakes	min	max	average	Standard deviation	50th percentile (median)	90th percentile	95th percentile
AS1	8151	0.1	36.7	8.6	3.8	8.7	13.1	14.2
AS2	6	7	15	11.2	2.9	11.5	14.5	14.8
AS3	747	0	32.2	8.6	3.6	8.8	12.1	13.3
AS4	185	0.3	34	11	5.5	9.9	18.3	22.1
AS5	10438	0	25.2	9.2	4.5	8.9	15.2	15.8
AS61	1930	0	18.7	6.9	2.9	7.1	10.4	11.2
AS62	1585	0	23.4	5.0	3.2	4.9	8.5	10.5
AS7	23	5	22	9.8	4.2	9.0	14.8	15.9
AS8	81	0.1	10.9	6.7	2.3	6.9	9.2	9.7
AS9	98	0.2	40	10.1	5.9	10	16.4	17.4
AS10	34	0	18.1	7.5	4.4	9.0	11.1	12.9
B1	134	1.1	51.1	17.3	7.8	16.6	26.1	30.7
B2	237	0.1	35.2	8.2	5.2	7.8	13.9	16.5

B31	1		12.2	12.2	12.2	0	12.2	12.2	12.2
B32	9		5.9	13	9.3	1.9	9.0	11.4	12.2
B4	29		0.7	32	9.0	6.2	8.0	11.4	20.8
B5	5		0	20.3	9.9	7.9	8.0	18.2	19.2
B6	0								

385 **Table 4: Earthquake depth statistics per area source zone with H_KPN18 catalogue (min, max, average, standard deviation, 50th, 90th, 95th percentile are in [km]).**
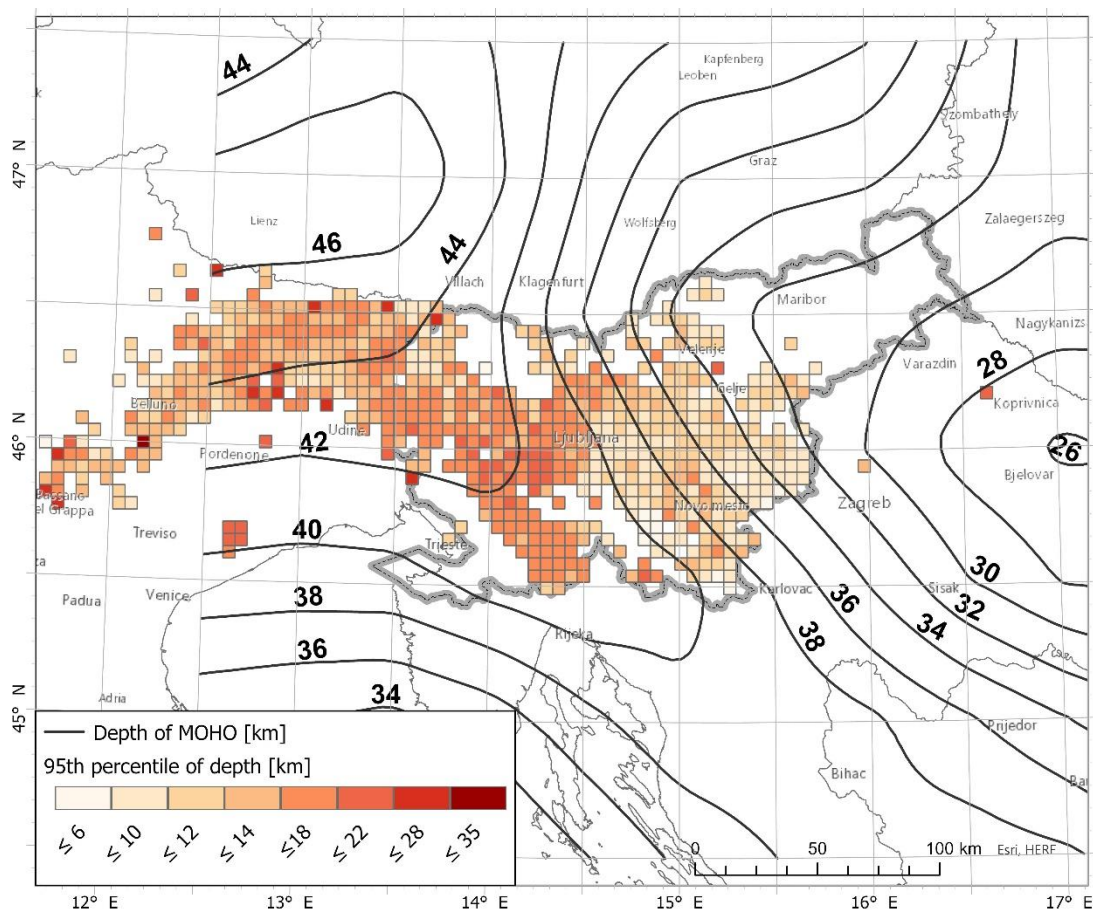
Area source	No. of earthquakes	min	max	average	Standard deviation	50th percentile (median)	90th percentile	95th percentile
AS1	257	0.4	51	9	5.4	9	13.4	15
AS2	10	7	18	9.7	3.3	8	14.4	16.2
AS3	55	1.5	22	9.8	4.4	8.6	15.2	17.6
AS4	97	0.3	33	10.3	5.4	10	17	18.4
AS5	222	0.5	99	9.8	9.4	8.1	15.7	19
AS61	58	1	18.3	7.6	4	7	13.2	16.1
AS62	186	0.1	26	8.5	5.7	6.9	18.2	19.9
AS7	77	4	22	7.8	2.5	8	10	11
AS8	28	4.4	15.6	8.7	2.2	8	12	12.1
AS9	140	0.1	30	10.8	6.2	10	18.1	21.1
AS10	31	3.3	29.6	12	7	11.6	19.4	25.3
B1	11	1	18.3	11	5.9	10	18.3	18.3
B2	8	0.9	11	6.2	3.6	5	10.5	10.8
B31	0							
B32	19	3	16	8.1	3	8	11.4	13.3
B4	60	1	49	8	5.9	8	10	11
B5	35	0.1	17	8.4	3.1	8	13.1	14.1
B6	1	7	7	7	0	7	7	7

Figure 5: The spatial distribution of 95th percentile of depth from IR18 catalogue earthquakes in 5x5 km² cells. Only cells containing at least four earthquakes are shown. Contours represent the depth of Mohorovičić discontinuity (Brückl et al., 2007; Grad et al., 2009).
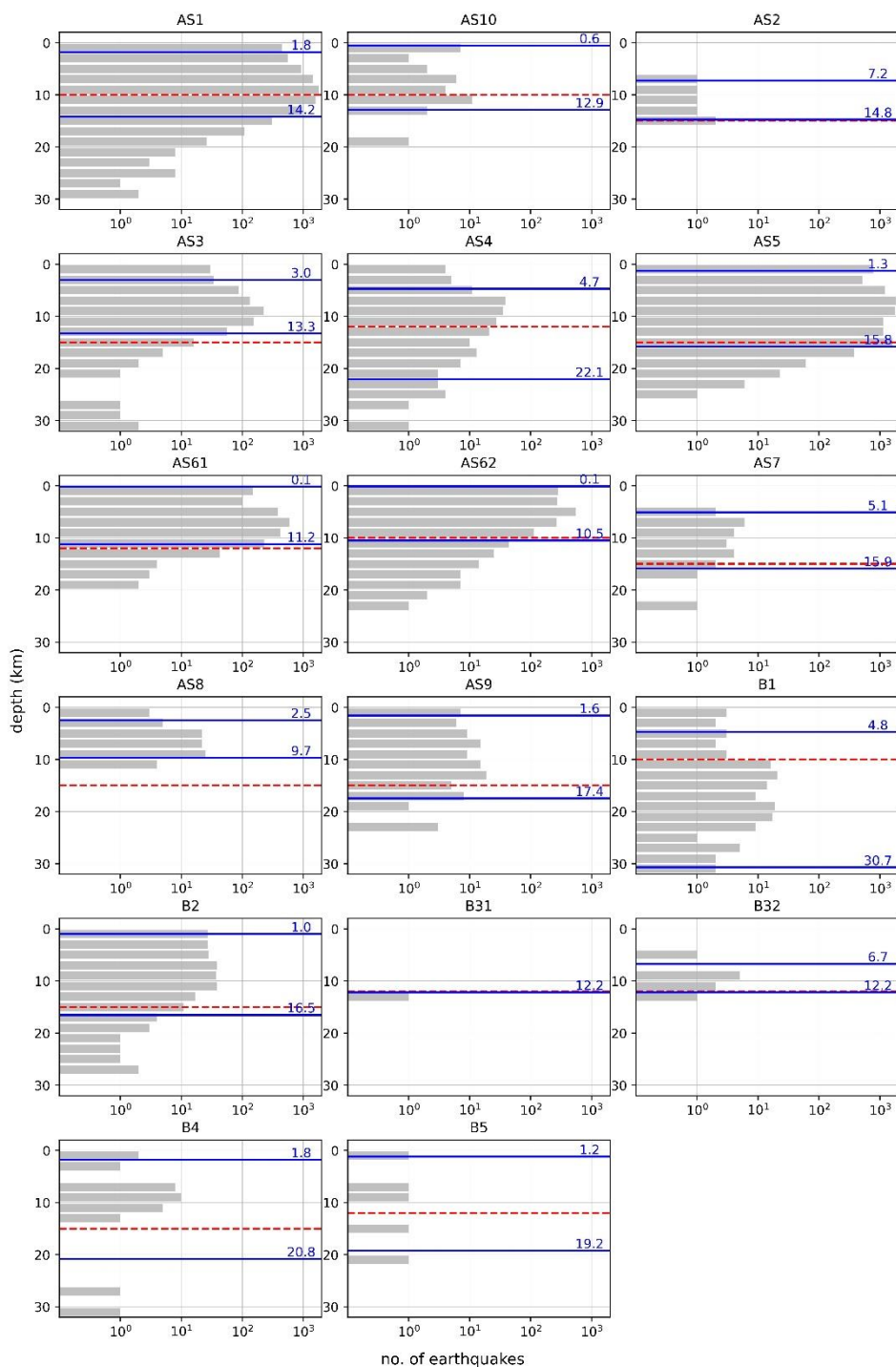
Figure 6: Earthquakes depth distribution per area source in IR18 catalogue (blue lines represent 5th and 95th percentile in [km] respectively), and the red dashed line represents the geological lower depth estimate. The B6 South Hungary area source contains no earthquakes. The scale for the number of earthquakes is logarithmic.

Table 5: Assigned final values of upper and lower seismogenic depth and hypocentral depth for A model.

| Area source	Area source name	Lower depth geological [km]	Lower depth seismological [km]	Final lower depth [km]	Hypocentral depth [km]	Upper depth [km]
AS1	Friuli	10	15	15	9	0
AS2	Molltal	15	16	16	8	0
AS3	Periadriatic	15	18	18	9	0
AS4	Outer Dinarides	12	22	22	10	0
AS5	Dinarides	15	19	19	8	0
AS61	Posavje	12	16	16	7	0
AS62	Gorjanci	10	19	19	7	0
AS7	Mur-Murz-VBTF	15	16	16	8	0
AS8	Labot	15	12	15	8	0
AS9	Inner Dinarides	15	21	21	10	0
AS10	Mid-Hungarian	10	19	19	12	0
B1	North Adriatic	12	31	31	10	0
B2	North Friuli	15	17	17	5	0
B31	Carinthia 1	12	16	16	8	0
B32	Carinthia 2	12	13	13	8	0
B4	North Alps	15	21	21	8	0
B5	Styria	12	19	19	7	0
B6	South Hungary	15	19	19	12	0

400
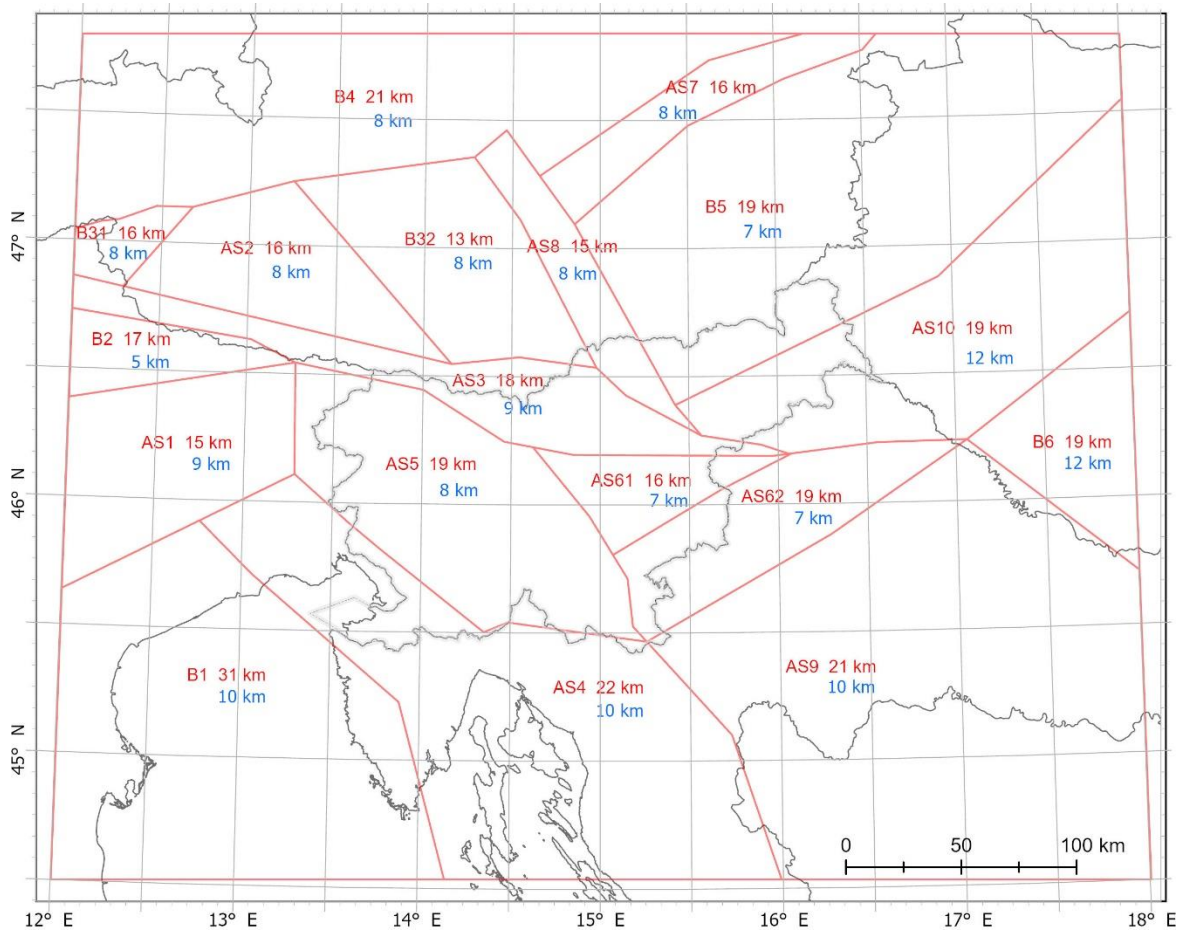
Figure 7: Area sources lower seismogenic depth (red colour text) and hypocentral depth (blue colour text).

3.2. Seismic moment rate calculation

405 We calculated the seismic moment rate $\dot{M}_{seis}$ from different complete earthquake sub-catalogues of KPN2018 using Eq. (4). We have varied the threshold magnitude m_t 3.8 and 4.1, according to the completeness year 1875, m_t 4.5 for the complete sub-catalogue since 1850, and m_t 5.1 for the complete sub-catalogue since 1840. Such threshold magnitudes were chosen because moment magnitude m_w strongly depends on the conversion from the intensities (m_w= 3.8 corresponds to intensity V EMS-98, 4.1 to intensity V-VI, 4.5 to intensity VI, 5.1 to intensity VII, and 5.6 to intensity VIII). The total annual number α_0 of

410 earthquakes above m_t for complete sub-catalogues is given in Table 6. For each complete sub-catalogue, we investigated the parameter space of β and M_c for a tapered Gutenberg-Richter distribution and selected the corner magnitude m_c where the peak of the likelihood function is found (see Jackson & Kagan, 1999; Bird & Kagan, 2004 for the formal statement of the likelihood function and applications at the global scale).

Natural Hazards
and Earth System
Sciences
Discussions

EGU

415 **Table 6: Corner magnitudes for four complete sub-catalogues.**

m_t	Year of completeness	α_0	m_c
3.8	1875	6.92	6.52
4.1	1875	3.19	6.22
4.5	1850	1.82	6.72
5.1	1840	0.43	6.62

In the first sensitivity analysis (Table 7(a)), the corner magnitude is fixed to 6.7, which is the best estimate of maximum magnitude for the largest part of Slovenian territory in A model, and is also the best estimate of maximum magnitude in P model (Šket Motnikar et al., 2022). The corresponding corner moment M_c was calculated using Eq. (3). We varied the

420 parameter β approximately in the range, determined by Bird and Kagan (2004) for continental convergent boundaries, and Carafa et al. (2017) for compressional and strike-slip faults. The value of the shear modulus is 35.2 GPa (Carafa et al, 2017). Thus we calculate the $\dot{M}_{seis}$ [1E+17 Nm/year] for various β and m_t (Table 7a and Fig. 8(a)).

In the second sensitivity analysis (Table 7(b)), besides the varying parameter β, we also varied the parameter m_c as obtained from Table 6.

425

Table 7. The seismic moment rate $\dot{M}_{seis}$[1E+17 Nm/year] for various β and m_t. Table 7(a): fixed m_c as m_{max} (6.7); Table 7(b): m_c varies according to different m_t as computed (Table 6).

(a)

Year of compl.	β m_t	0.55	0.57	0.59	0.61	0.63	0.65	0.67	0.69	0.71	0.77	0.83
1875	3.8	6.19	5.30	4.56	3.93	3.39	2.94	2.56	2.24	1.96	1.37	1.04
	4.1	5.05	4.41	3.87	3.41	3.00	2.66	2.36	2.11	1.89	1.41	1.13
1850	4.5	6.16	5.54	4.99	4.51	4.09	3.73	3.40	3.12	2.88	2.33	2.03
1840	5.1	4.56	4.28	4.02	3.79	3.58	3.40	3.23	3.09	2.97	2.72	2.69

(b)

Year of compl.	β m_c	0.55	0.57	0.59	0.61	0.63	0.65	0.67	0.69	0.71	0.77	0.83
1875	6.52	4.68	4.06	3.53	3.08	2.70	2.37	2.08	1.84	1.64	1.19	0.93
	6.22	2.39	2.17	1.96	1.78	1.63	1.49	1.37	1.26	1.17	0.96	0.85

| 1850 | 6.72 | 6.35 | 5.70 | 5.14 | 4.64 | 4.20 | 3.82 | 3.48 | 3.19 | 2.93 | 2.37 | 2.06 |
| 1840 | 6.62 | 4.03 | 3.80 | 3.59 | 3.41 | 3.24 | 3.09 | 2.96 | 2.84 | 2.74 | 2.56 | 2.57 |

430   **3.2.1. Comparison of seismic and tectonic moment rates for all FS**

Besides the calculations of the seismic moment rate $\dot{M}_{seis}$ (based on seismicity and with various β, m_c, and m_t), we calculated also the tectonic moment rate $\dot{M}_{tect}$. For seismogenic fault sources from EDSF (Basili et al., 2013), the seismic coupling c is not applied. For the remaining 67 FS, we estimated five alternatives: fixed value c = 1, a fixed value of 0.7, and three (upper, mean, and lower) individually determined c values, according to Table 2 (as described in Sec. 2). Using five alternatives of
435   seismic coupling and applying Eq. (5), we calculated five alternatives of $\dot{M}_{tect}$ for all FS, and summed them up. The overall tectonic moment rates for all five alternatives are shown in Table 8 and presented with a red line in Fig. 8a and 8b, corresponding to the seismologically determined seismic moment rate from Table 7a and 7b respectively.

Table 8. The sum of tectonic moment rates of all FS $\dot{M}_{tect}$ [in 1E+17 Nm/years] for five alternative approaches of seismic coupling.
440   **Seismic coupling was not applied to FS taken from EDSF (Basili et al., 2013).**

Seismic coupling c = 1	Seismic coupling c = 0.7	Individual coupling (Table 2, max estimate)	Individual coupling (Table 2, mean estimate)	Individual coupling (Table 2, min estimate)
8.29	6.31	4.15	3.76	3.37

Natural Hazards
and Earth System
Sciences

Open Access

Discussions

EGU
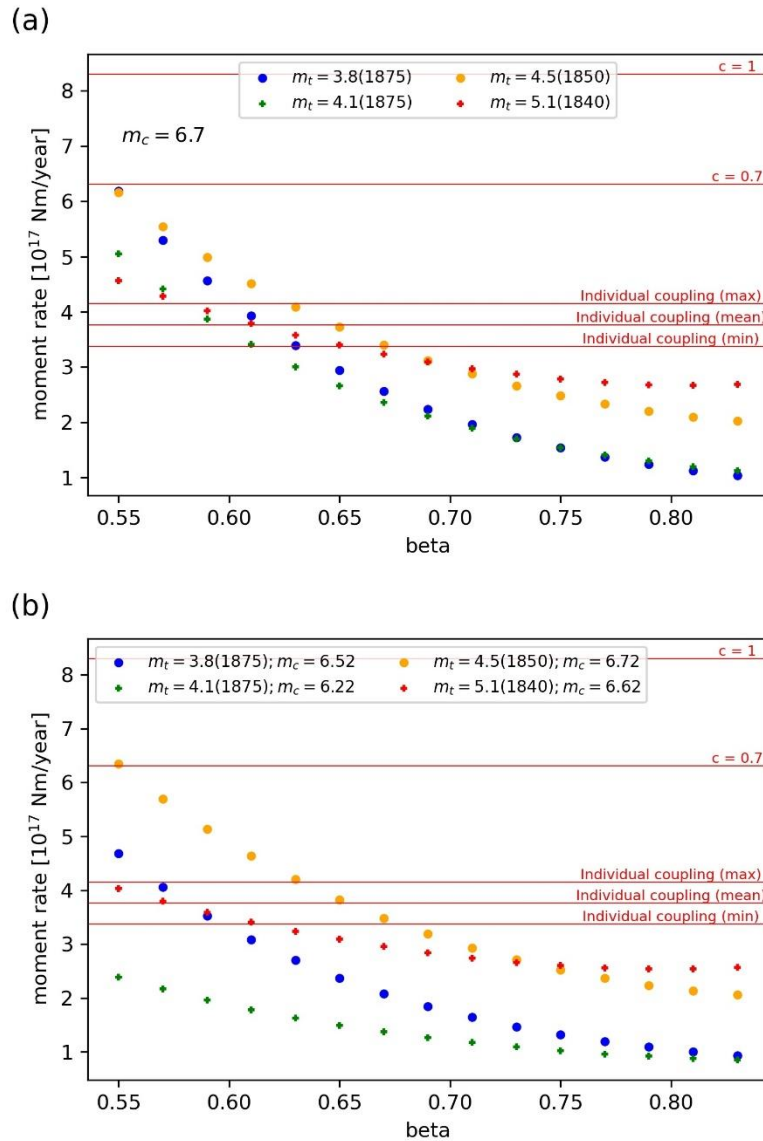
Figure 8: Comparison of seismologically determined seismic moment rates $\dot{M}_{seis}$ (dots) and tectonic moment rates $\dot{M}_{tect}$ (red lines) for different threshold magnitude m_t and different year of completeness from catalogue KPN2018 depending on the slope of the moment-frequency relation value β. Figure 8a: fixed m_c = 6.7; Figure 8b: m_c varied (values in Table 6).

We compared seismologically determined seismic moment rates $\dot{M}_{seis}$ for different threshold magnitudes m_t and different year of completeness of catalogues with tectonic moment rates. The results (Tables 7 and 8, and Fig. 8) show that the application of coupling is justified and the choice of method (after Carafa et al., 2017) is appropriate. The fit is the best between the seismic moment rates for m_t 4.5 (yellow dots in Fig. 8) and for seismic couplings (mean estimate) after Carafa et al., 2017. Therefore,

a higher weight (70 %) is given to the "Carafa c" branch in PSHA, complementary to the branch that corresponds to the fixed c = 0.7 (weight 30 %).

3.2.2. Comparison of seismic and tectonic moment rates for FS, grouped by area source zones

455 A comparison of seismic moment rates calculated from the catalogue (threshold magnitude m_t 4.5, year of completeness 1850, corner magnitude m_c 6.7) vs. tectonic moment rates calculated from fault slip-rates is done for earthquakes and faults grouped by AS (Fig. 2).

Some representative results are shown in Fig. 9. For Posavje and Gorjanci areas the moment rates from seismicity since 1850
460 are way over the moment rates calculated from fault slip rates. This might suggest some hidden active structures that were not recognised and included in our fault-based SSC model. On the other hand, the tectonic moment rate is higher than the moment rate from seismicity in the Periadriatic zone. This could indicate very aseismic movement in the area. The moment rates from Dinarides and Outer Dinarides area zones show good agreement with the chosen coupling values. All FS in the Friuli zone are from EDSF (Basili et al., 2013), which is also reflected in graphs (c = 1). Results are a good indicator of areas, where future
465 investigations of active structures are necessary. They also indicate areas, where future analysis and estimation of slip rates and seismic coupling should be performed more in detail.
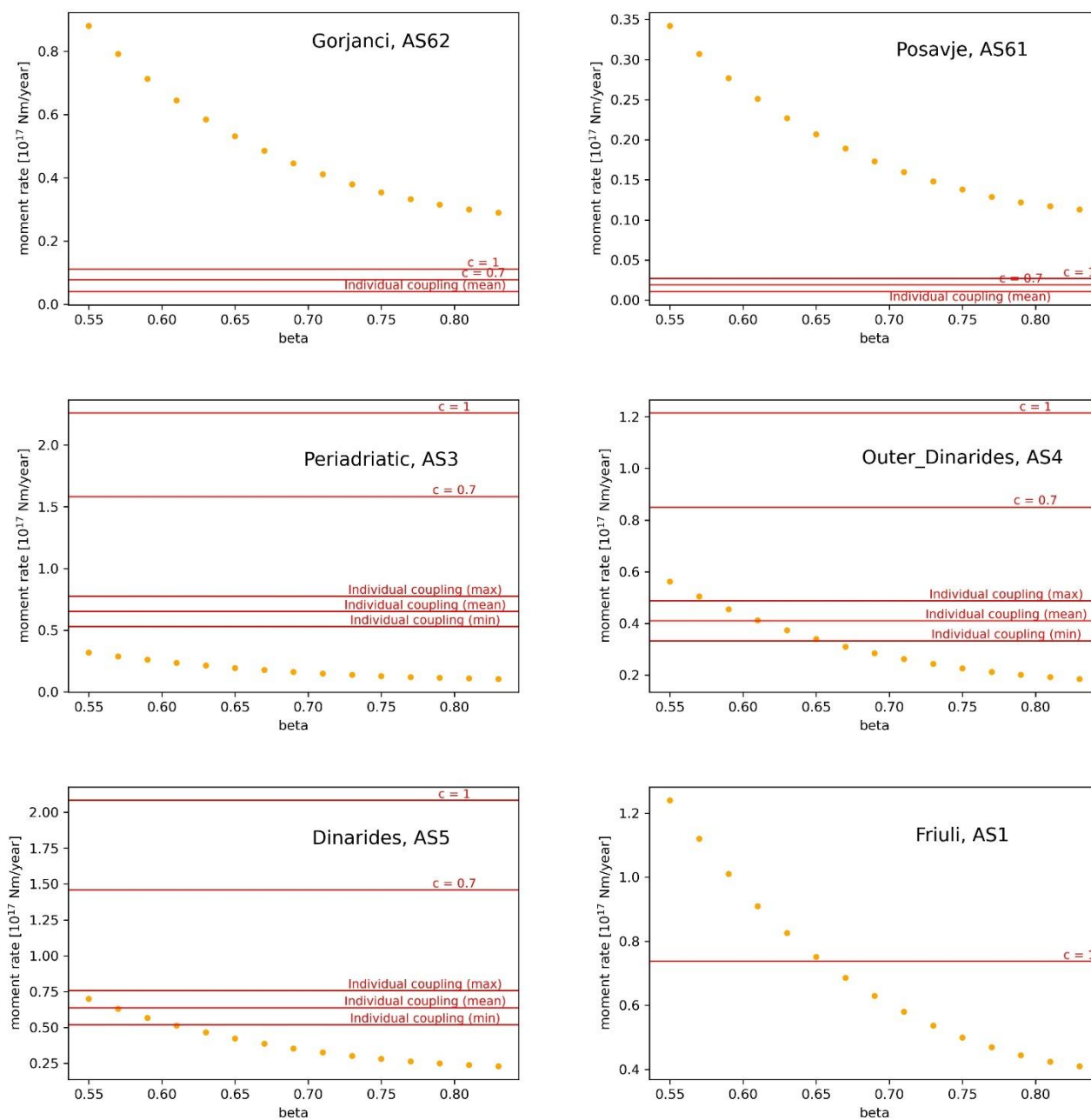
470 **Figure 9: Comparison between seismologically determined seismic moment rate $\dot{M}_{seis}$ (yellow dots) of individual area source zones and tectonic moment rate $\dot{M}_{tect}$ (red lines) for FS, grouped by area source zones. Seismic moment rate from the complete KPN2018 catalogue, m_t 4.5, year of completeness 1850, and corner magnitude m_c 6.7.**

26

3.3. Slip rate and seismic coupling

475 The seismic coupling in Carafa et al. (2017) was determined for faults grouped according to their kinematics. In that case, the authors didn't use the fault slip rates as direct input because they were often missing or with overlooked uncertainty (Carafa et al., 2022). Instead, after anticipating and discounting short-term transients (Carafa and Bird, 2016), the GNSS-derived horizontal strain rate tensor was a good proxy for them and was used in seismic coupling estimation by Carafa et al. (2017). In general, GNSS derived velocity field represents the bulk displacements; seismic slip and aseismic slip, off-fault

480 accumulation, and non-tectonic displacement. In our case, slip rate estimates refer to the total slip, including the aseismic part (Atanackov et al., 2021) and GNSS derived data represent only a minor part of input data for slip rate estimation.

To check the assumption that our estimation of the total slip rate and GNSS measurements do not differ much, we considered the largest parallel faults between (and including) Črni Kal – Palmanova and Idrija FS (area indicated with a dashed rectangle in Fig. 11) that is a proxy of the displacement in N-S direction (1,94 mm/year) which is the approximate regional stress

485 direction. Five of the seven chosen FS have the probability of activity 1. The other two fault sources have a probability of 0.7 (Buzet) and 0.5 (Divača). Considering Buzet and Divača as not active, which presents the lower limit of our estimate, the budget of slip in the N-S direction is reduced to 1,79 mm/year. The area was chosen also because in the western part of Slovenia, the GNSS network is the densest and therefore the observations are the most reliable. The most up-to-date review of measured GNSS vectors is available in the paper by Serpelloni et al. (2016). Interpolated velocity field of northward

490 movements between Črni Kal – Palmanova and Idrija Faults show a decrease of velocity towards the North from approximately 2.5 mm/year in the Slovenian Istra to 1.0-1.5 mm/year at the southern margin of the Julian Alps. Based on the GNSS data the total N-S horizontal shortening absorbed by the faults in this area at present is therefore approximately 1.0-1.5 mm/year. Since the interpolation is done on a relatively small number of GNSS data points, the estimated shortening is relatively poorly constrained and may be over- or under- estimated. The N-S shortening across the whole of Slovenia is estimated at 2-4 mm/year

495 according to the GNSS data from an earlier study (Weber et al., 2010).

The calculated N-S components of the estimated slip of the chosen faults are in Table 9. The comparison with the results of Serpelloni et al. (2016) and Weber et al. (2010) shows that the regional geologic and geodetic shortening rates are comparable.

Table 9: Sum of N-S components of fault movements along the largest faults in western Slovenia.

Name	Fault ID	Dip	Rake	Strike	Slip [mm/year]	N-S projection of SR [mm/year]
Buzet	SS.SI-002	20	90	310	0.050	0.036
Črni Kal - Palmanova	SS.SI-006	25	90	315	0.200	0.128
Divača	SS.SI-011	80	160	305	0.200	0.118
Raša	SS.SI-014	85	170	315	0.700	0.495
Predjama-Avče	SS.SI-019	80	170	310	0.700	0.459
Idrija	SS.SI-022	85	165	310	1.000	0.638

| Ravne	SS.SI-025	80	170	310	0.100	0.066
					Sum [mm/year]:	1.940

500

The seismic coupling value calculated following Carafa et al. (2017) depends on the seismogenic thickness of the given fault source and its fault kinematics. The mean estimate of seismic coupling ranges from 0.8 for Divača (SS.SI-011) shallow strike-slip fault to 0.24 for deep Periadriatic E and W faults (SS.SI-056a, b). The uncertainty in the seismic coupling of slip rates is

505 handled with two logic-tree branches. The first branch is based on the literature data (Table 1) and considers fixed 0.7 of the slip rates to be seismically coupled. The second branch is based on individual values of seismic coupling for each fault, calculated after Carafa et al. (2017). The weight of the first branch is 30 % and the weight of the second branch is 70 % (Šket Motnikar et al., 2022). The seismic coupling was applied to all but 22 FS from EDSF (Basili et al., 2013). The final estimate of seismic coupling ranges from 0.77 to 0.38 (Fig. 10).

510

The uncertainty in slip rate is modelled in three logic tree branches for lower, best, and upper alternative values. The seismic part of slip rate (best) estimates ranges from 0.01 mm/year to 0.65 mm/year. (Fig. 11). The highest seismic part of slip rates in Slovenia is estimated for the Sava (E and W) and Idrija faults with 0.43 mm/year and 0.42 mm/year respectively. The results of the slip rate estimates and seismic coupling for all FS in the F model are available in the Pangaea portal, columns *Min slip*

515 *rate, Max slip rate, Best estimate slip rate, Seismogenic layer thickness, Coupled thickness_Carafa mean, Coupled thickness_Carafa min, Coupled thickness_Carafa max, Seismic coupling_Carafa mean, Seismic coupling_Carafa min, Seismic coupling_Carafa max, Seismic coupling* (Atanackov et al., 2022).
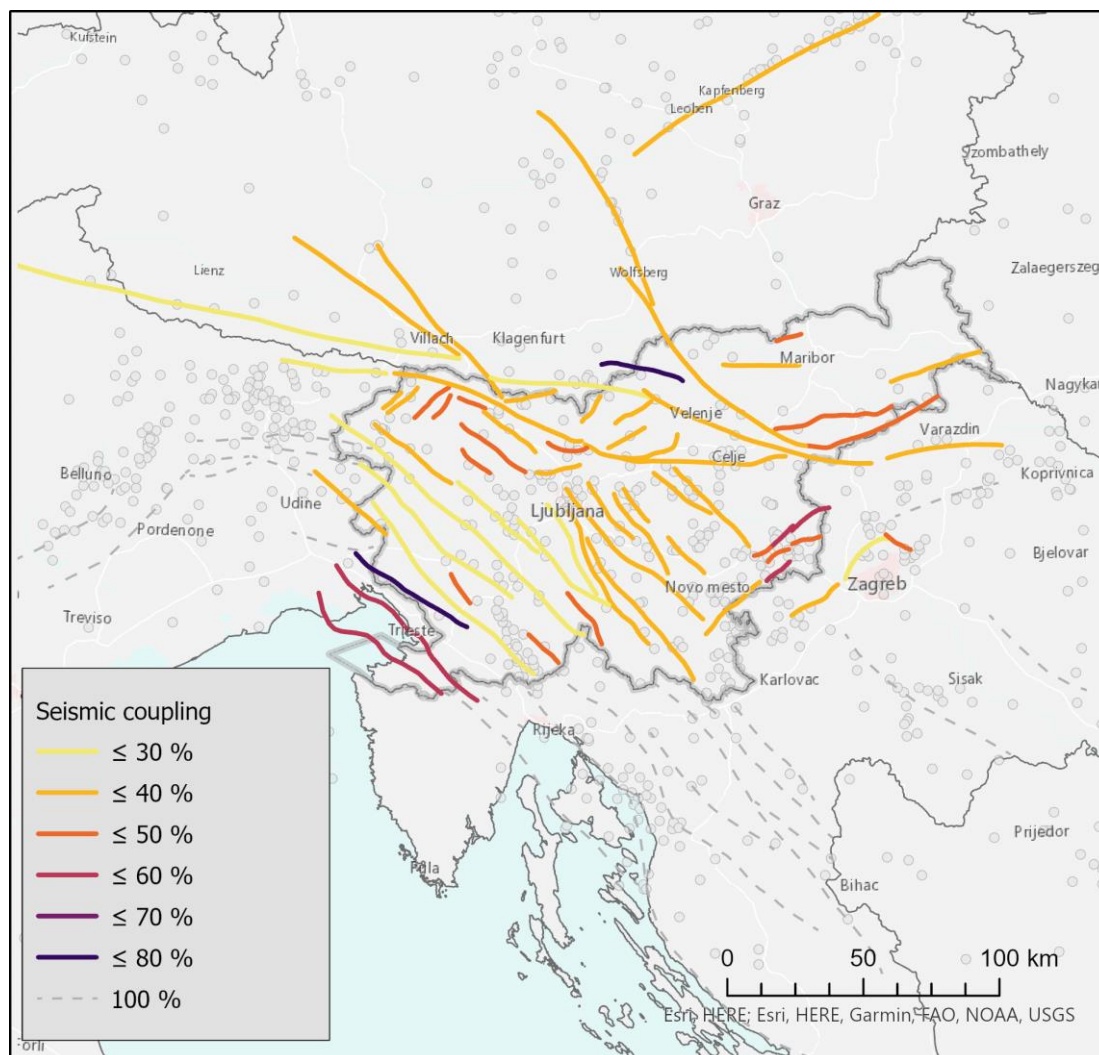
Figure 10: Individual seismic coupling factor for each fault seismic source.

520
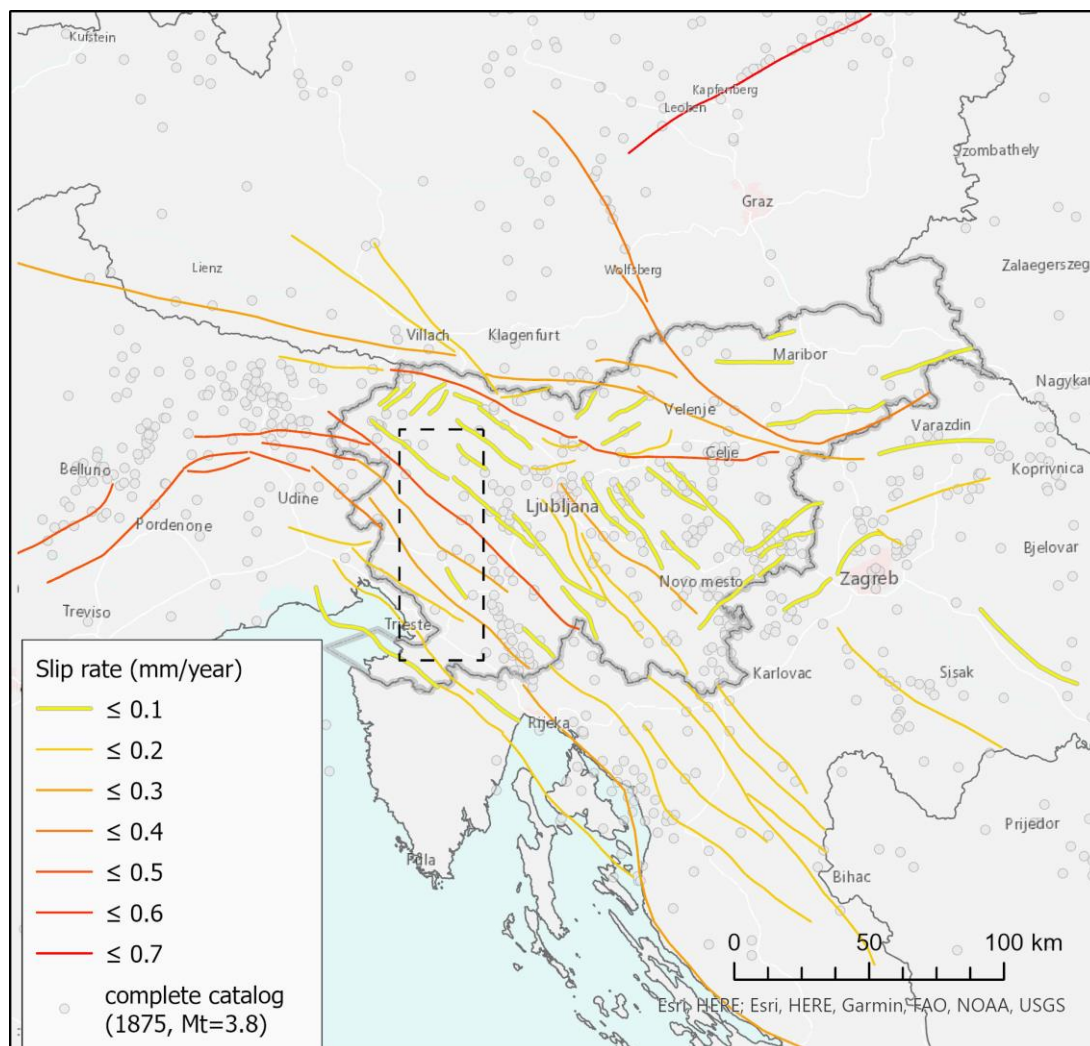
Figure 11: The seismic part of the slip rates on individual faults as considered in the final PSHA calculation. The dashed rectangle indicates the area of slip rate analysis (Table 9).

3.4. Comparison of total activity rate in the A, F, and P model

The three global seismic source models (A, F and P) have different purposes and assumptions, but each of the models should be complete by itself. It is expected that they produce different seismic hazard values and different areas of the highest values, although we cannot tell in advance which will give the highest hazard values and where. However, if one model significantly differs from others, it is recommended to analyze the most influential parameters and find reasons for such a difference. In Table 10, the total activity rate (annual number of all earthquakes above magnitude 0 in the influential area) of the three global models is compared. In addition, four branches of the fault model (active, probable, potential, and questionable) are considered separately, and their weights are taken into account in the total values.

As expected, the difference between the A and P models is very small because both total activity rates are based on counting

earthquakes in the complete (declustered) catalogue (from 1875, m_t=3.8). The difference of 0.5 % results from smoothing

540   around borders of the influence area, and on different m_{max} values in A and P models.

The F model gives a different picture of seismicity than the catalogue because the period of the complete catalogue is shorter

than the return period of the largest possible magnitude of fault sources. Activity rate in the F model is converted from slip

rate using Youngs and Coppersmith (1985) relationship, or (equivalently) the fourth model in (Bungum, 2007), Eq. (10), where

545   the activity rate is explicitly expressed as:

$$N_4(m^0) = \frac{\mu A_f S(d-b)\left[1-e^{-\beta(m^u-m^0)}\right]}{bM^u e^{-\beta(m^u-m^0)}},$$ (6)

where $A_f = LW$ is fault area depending on depth and dip, S is slip rate, m^u is maximum magnitude, m^0 is lower bound magnitude,

and M^u, d, b, and μ are constants. Details and values of constants are provided in Youngs & Coppersmith (1985) (Eq. (11)).

550   When the slip rates are converted to activity rate, the total activity rate of the F model is approximately 62 % higher than the

A model. We know that this is unrealistic because the slip rates estimated by Atanackov et al (2021, 2022) contain also the

aseismic part and large events post-seismic parts. When the seismic coupling is 0.7, the total activity rate of the F model is

approximately 24 % higher than the other two models A and P. When the seismic coupling is calculated after Carafa et al.,

(2017) individually per each fault source, the total activity rate of the F model is around 23 % lower than the other two models.

555

In the hazard calculation, we used two branches of seismic coupling with weights 70 %, and 30 %, respectively for coupling

c = 0.7, and for coupling calculated after Carafa et al. (2017). Taking into account the two weighted branches, the total activity

rate of the F model (grey line in Table 10) is around 9 % lower than the other two models A and P. This could be partly

explained by the fact that some seismicity is generated on smaller faults that are not part of our F model. Also, the fault source

560   buffers do not cover the whole area of observation. Therefore, in the hazard calculation, the F model is complemented with

the background seismicity.

Despite the very different approaches of estimation and very different time spans of geological vs. seismological data, the

seismic activity of all three global seismic models shows less than a 10 % difference, which does not indicate the need to revise

565   the models.

Table 10: Comparison of the total activity rate (annual number of earthquakes above magnitude 0 calculated from complete catalogue m_w>=3.8, 1875 on) in seismic source models. The middle column denotes weight according to the type of fault source activity (active, probably, potentially, or questionably active). In the F model, two alternatives of seismic coupling (c = 0.7, and mean
570   **seismic coupling after Carafa et al. (2017) are considered (grey line).**

Model	Weighted N(0) of earthquakes	Weight according to the fault activity	Total N(0) of earthquakes
A	39017		
P	39234		
F total (seismic coupling c = 1)	63468		78307
F active only	42496	1	42496
F probable only	12106	0.7	17294
F potential only	8473	0.5	16947
F questionable only	393	0.25	1571
F total (seismic coupling c = 0.7)	48544		60770
F active only	31557	1	31557
F probable only	9292	0.7	13275
F potential only	7419	0.5	14838
F questionable only	275	0.25	1100
F total (mean seismic coupling after Carafa)	30002		39298
F active only	17883	1	17883
F probable only	5534	0.7	7906
F potential only	6414	0.5	12828
F questionable only	170	0.25	681
F total as calculated in the hazard model (70 % for 0.7 seismic coupling, and 30 % for seismic coupling after Carafa et al. (2017)	35565		

4. CONCLUSION

The characterization of seismogenic sources and the process of determining the seismic coupling require knowledge of the seismogenic lithosphere's thickness, which is bounded by upper and lower seismogenic depth. This study, based on two updated earthquake catalogues for the transition zone between the Alps, Dinarides and Pannonian Basin, explores the

575   variability of seismogenic depth and seismic coupling to be included in the new Slovenian seismic hazard model. The detailed analysis of seismogenic depth is based on geological expert knowledge and on a seismological approach by studying the depth distribution of earthquakes for each FS and AS separately. The seismogenic lower depth for FS is in the range of 5 km (SS.SI078 Northern Karavanke thrust fault) to 20 km (SS.SI-056a,b Sava W and E faults). The estimated values of seismogenic lower depth for AS are higher and reflect the use of the historical H_KPN18 catalogue. The values for AS are in the range of

580 13 km to 31 km. The upper seismogenic depth for FS and AS is estimated from known geological and geophysical data interpretations. The upper seismogenic depth value for FS is in the range from 0 km to 6 km while it is 0 km for all AS. Seismogenic depth determined from the analysis of the earthquake catalogues depends greatly on the velocity model used to locate earthquakes. As Rajh et al. (2022) and Rajh (2022) demonstrated, an improved velocity model in our study area can have a profound effect on earthquake locations, especially their depths. The earthquake hypocentres relocated with the new

585 models were on average shallower by about 2-3 km. This could close the gap between the geological and seismological lower seismogenic depth estimates even further. However, at the time of this study, the models were not readily available.

Seismic coupling determines the proportion of slip rate that directly affects the annual earthquake rate in a given fault source and is therefore of great importance to PSHA. We used two approaches for the determination of seismic coupling. We reviewed

590 the existing literature and adopted the best assessment for the studied area and the chosen value of 0.7 was used as one logic tree branch in PSHA. In the second branch, the seismic coupling was estimated individually for each FS following Carafa et al. (2017). The values of seismic coupling following Carafa et al. (2017) depend upon the seismogenic layer thickness of the given fault source and the fault kinematics. The estimated seismogenic thickness for FS ranges from 5 km to 20 km and the weighted average of both estimates of seismic coupling ranges from 0.77 to 0.38. The values thus obtained were compared in

595 terms of seismic moment rates for the whole studied area and for individual FS grouped by AS. The sum of tectonic moment rates of all FS for alternative approaches of seismic coupling ranges from 3.76E+17 Nm/year for the mean estimate of individual coupling to 8.29E+17 Nm/year for c=1. We also compared the total activity rate based on the complete earthquake catalogue with the rate based on the seismic part of slip rates in FS and seismic activity of all three global seismic models shows less than 10 % difference. These comparisons complete our analyses of the seismic coupling estimation to national-

600 scale high-quality datasets.

Data availability

The data used in this manuscript are published as a dataset identified by the DOI https://doi.org/10.1594/PANGAEA.940100, which is openly accessible.

605

Author contributions

All authors contributed to the study's conception and design. The first draft of the manuscript was written by PZ and BŠM, and all authors read, commented, and improved previous versions of the manuscript. All authors approved the final manuscript.

610 *Competing interests*

The authors declare that they have no conflict of interest.

Acknowledgments

Natural Hazards
and Earth System
Sciences
Discussions

Open Access

EGU

5.   REFERENCES

Aki, K.: Generation and propagation of G waves from the Niigata earthquake of June 16, 1964: Part 2. Estimation of earthquake moment, released energy and stress drop from the G wave spectra, Bull. Earthq. Res. Inst., Univ. Tokyo, 44, 73-88, 1966.

ARSO: Digital earthquake database for Slovenia, Agencija Republike Slovenije za okolje - Slovenian Environment Agency,
620   Ljubljana, Slovenia, 2018.

ARSO: Design ground acceleration map of Slovenia, Agencija Republike Slovenije za okolje - Slovenian Environment Agency, Ljubljana, Slovenia, http://www.arso.gov.si/potresi/potresna%20nevarnost/projektni_pospesek_tal.html, last access: 20. April 2022, 2001.

Atanackov, J., Jamšek Rupnik, P., Jež, J., Celarc, B., Novak, M., Milanič, B., Markelj, A., Bavec, M., and Kastelic, V.:
625   Database of Active Faults in Slovenia: Compiling a New Active Fault Database at the Junction Between the Alps, the Dinarides and the Pannonian Basin Tectonic Domains, Front. Earth Sci., 9:.604388. 10.3389/feart.2021.604388, https://doi.org/10.3389/feart.2021.604388, 2021.

Atanackov, J., Jamšek Rupnik, P., Zupančič, P., Šket Motnikar, B., Živčić, M., Čarman, M., Milanič, B., Kastelic, V., Rajh, G., and Gosar, A.: Seismogenic fault and area sources for probabilistic seismic hazard model in Slovenia, PANGAEA,
630   https://doi.org/10.1594/PANGAEA.940100, 2022.

Bajc, J., Aoudia, A., Sarao, A., and Suhadolc, P.: The 1998 Bovec-Krn mountain (Slovenia) earthquake sequence, Geophysical Research Letters, 28 (9), 1839-1842, https://doi.org/10.1029/2000GL011973, 2001.

Baker, J. W., Bradley, B. A., and Stafford, P. J.: Seismic Hazard and Risk Analysis, Cambridge University Press, Cambridge, England, https://doi.org/10.1017/9781108425056, 2021.

635   Basili, R., Danciu, L., Beauval, C., Sesetyan, K., Pires Vilanova, S., Adamia, S., Arroucau, P., Atanackov, J., Baize, S., Canora, C., Caputo, R., Carafa, M. M. C., Cushing, E. M., Custódio, S., Demircioglu Tumsa, M. B., Duarte, J. C., Ganas, A., García-Mayordomo, J., Gómez de la Peña, L., Gràcia, E., Jamšek Rupnik, P., Jomard, H., Kastelic, V., Maesano, F. E., Martín-Banda, R., Martínez-Loriente, S., Neres, M., Perea, H., Šket Motnikar, B., Tiberti, M. M., Tsereteli, N., Tsironi, V., Vallone, R., Vanneste, K., Zupančič, P., and Giardini, D.: The European Fault-Source Model 2020 (EFSM20): geologic input data for the
640   European Seismic Hazard Model 2020, submitted to NHESS Special issue Harmonized seismic hazard and risk assessment for Europe, 2023.

Basili, R., Kastelic, V., Demircioglu, M. B., Garcia Moreno, D., Nemser, E. S., Petricca, P., Sboras, S. P., Besana-Ostman, G. M., Cabral, J., Camelbeeck, T., Caputo, R., Danciu, L., Domac, H., Fonseca, J., García-Mayordomo, J., Giardini, D., Glavatovic, B., Gulen, L., Ince, Y., Pavlides, S., Sesetyan, K., Tarabusi, G., Tiberti, M. M., Utkucu, M., Valensise, G.,

645   Vanneste, K., Vilanova, S. and Wössner J.: The European Database of Seismogenic Faults (EDSF) compiled in the framework of the Project SHARE, http://diss.rm.ingv.it/share-edsf/, doi: 10.6092/INGV.IT-SHARE-EDSF, 2013.

Bird, P., and Kagan, Y. Y.: Plate-tectonic analysis of shallow seismicity: Apparent Boundary Width, Beta, Corner Magnitude, Coupled Lithosphere Thickness, and Coupling in Seven Tectonic Settings, B. Seismol. Soc. Am., 94 (6), 2380–2399, https://doi.org/10.1785/0120030107, 2004.

650   Bressan, G., Gentile, G. F., Perniola, B., and Urban, S.: The 1998 and 2004 Bovec-Krn (Slovenia) seismic sequences: aftershock pattern, focal mechanisms and static stress changes, Geophys. J. Int., 179 (1), 231-253, https://doi.org/https://doi.org/10.1111/j.1365-246X.2009.04247.x, 2009.

Brückl, E., Bleibinhaus, F., Gosar, A., Grad, M., Guterch, A., Hrubcová, P., Keller, G. R., Majdański, M., Šumanovac, F., Tiira, T., Yliniemi, J., Hegedus, E., and Thybo, H.: Crustal structure due to collisional and escape tectonics in the Eastern Alps

655   region based on profiles Alp01 and Alp02 from the ALP 2002 seismic experiment, J. Geophys. Res., 112, B06308, https://doi.org/10.1029/2006JB004687, 2007.

BSHAP-2: Improvements in the Harmonized Seismic Hazard Maps for the Western Balkan Countries, SfP project number 984374, 2015.

Burrato, P., Poli, M. E., Vannoli, P., Zanferrari, A., Basili, R., and Galadini, F.: Sources of Mw 5+ earthquakes in northeastern

660   Italy and western Slovenia: An updated view based on geological and seismological evidence, Tectonophysics, 453, 157–176, http://dx.doi.org/10.1016/j.tecto.2007.07.009 , 2008.

Bus, Z., Grenerczy, G., Tóth, L., and Mónus, P.: Active crustal deformation in two seismogenic zones of the Pannonian region — GPS versus seismological observations, Tectonophysics, 474, Issues 1–2, 343-352, https://doi.org/10.1016/j.tecto.2009.02.045, 2009.

665   Carafa, M. M. C., Di Naccio, D., Di Lorenzo, C., Kastelic, V., and Bird, P.: A meta-analysis of fault slip rates across the central Apennines. Journal of Geophysical Research: Solid Earth, 127, e2021JB023252. https://doi.org/10.1029/2021JB023252, 2022.

Carafa, M., Valensise, G., and Bird, P.: Assessing the seismic coupling of shallow continental faults and its impact on seismic hazard estimates: A case-study from Italy, Geophys. J. Int., 209, 32-47, doi: 10.1093/gji/ggx002, 2017.

670   Carafa, M. M. C., and Bird, P.: Improving deformation models by discounting transient signals in geodetic data: 2. Geodetic data, stress directions, and long-term strain rates in Italy, J. Geophys. Res. Solid Earth, 121, 5557– 5575, doi:10.1002/2016JB013038, 2016.

Cornell, C. A.: Engineering seismic risk analysis, B. Seismol. Soc. Am. 58, 1583-1606, 1968.

Danciu, L., Nandan, S., Reyes, C., Basili, R., Weatherill, G., Beauval, C., Rovida, A., Vilanova, S., Sesetyan, K., Bard, P-Y.,

675   Cotton, F., Wiemer, S., and Giardini, D.: The 2020 update of the European Seismic Hazard Model: Model Overview, EFEHR Technical Report 001, v1.0.0, https://doi.org/10.12686/a15, 2021.

Natural Hazards
and Earth System
Sciences
Discussions

GEM: The OpenQuake-engine User Manual. Global Earthquake Model (GEM) OpenQuake Manual for Engine version 3.16.3, doi: 10.13117/GEM.OPENQUAKE.MAN.ENGINE. 3.16.3, 2022.

Gosar, A.: Review of geological and seismotectonic investigations related to 1998 Mw5.6 and 2004 Mw5.2 earthquakes in

680   Krn Mountains, Geologija, 62 (1), 61–73, doi:10.5474/geologija.2019.002, 2019a.

Gosar, A.: Review of seismological investigations related to 1998 Mw5.6 and 2004 Mw5.2 earthquakes in Krn Mountains, Geologija, 62 (1), 75–88, doi:10.5474/geologija.2019.003, 2019b.

Grad, M., Tiira, T., and ESC Working Group: The Moho depth map of the European Plate, Geophys. J. Int., 176, 279-292, doi: 10.1111/j.1365-246X.2008.03919.x, 2009.

685   Grützner, C., Aschenbrenner, S., Jamšek Rupnik, P., Reicherter, K., Saifelislam, N., Vičič, B., Vrabec, M., Welte, J., and Ustaszewski, K.: Holocene surface rupturing earthquakes on the Dinaric Fault System, western Slovenia, Solid Earth, 12, 2211–2234, https://doi.org/10.5194/se-12-2211-2021, 2021.

Guidarelli, M., Aoudia, A., and Costa, G.: 3-D structure of the crust and uppermost mantle at the junction between the Southeastern Alps and External Dinarides from ambient noise tomography, Geophysical Journal International, 211 (3), 1509-

690   1523, https://doi.org/10.1093/gji/ggx379, 2017.

Herak, M., Herak, D., and Orlić, N.: Properties of the Zagreb 22 March 2020 earthquake sequence – analyses of the full year of aftershock recording, Geofizika, 38, 93-116, https://doi.org/10.15233/gfz.2021.38.6, 2021.

INOGS: Bollettino della Rete Sismometrica del Friuli-Venezia-Giulia, Instituto Nazionale di Oceanografia e di Geofisica Sperimentale, Centro Ricerche Sismologiche (CRS), online http://www.crs.ogs.it/bollettino/RSFVG/, last access: 21. 7. 2023,

695   1977-2014.

Jackson, D. D. and Kagan, Y. Y.: Testable Earthquake Forecasts for 1999, Seismol. Res. Lett., 70 , 393-403, 1999.

Kapuralić, J., Šumanovac, F., and Markušić, S.: Crustal structure of the northern Dinarides and southwestern part of the Pannonian basin inferred from local earthquake tomography, Swiss J. Geosci., 112 (1), 181-198, https://doi.org/10.1007/s00015-018-0335-2, 2019.

700   Kagan, Y.Y.: Seismic moment distribution revisited: II. Moment conservation principle. Geophysical Journal International, 149, 731–754, 2002.

Kastelic, V.: Seismotectonic study of Ravne fault and 1998 and 2004 Upper Posočje earthquakes, Ph. D. Thesis, University of Ljubljana, Ljubljana, Slovenia, 112 pp, 2008.

Kastelic, V., Vrabec, M., Cunningham, D., and Gosar, A.: Neo-Alpine structural evolution and present day tectonic activity of

705   the eastern Southern Alps: the case of the Ravne Fault, NW Slovenia, J. Struct. Geol., 30 (8), 963-975, https://doi.org/10.1016/j.jsg.2008.03.009, 2008.

Lapajne, J. K., Šket Motnikar, B., and Zupančič, P.: Probabilistic Seismic Hazard Assessment Methodology for Distributed Seismicity, B. Seismol. Soc. Am., 93(6), 2502-2515, 2003.

Natural Hazards
and Earth System
Sciences
Discussions

Michelini, A., Živčić, M., and Suhadolc, P.: "Simultaneous inversion for velocity structure and hypocenters in Slovenia."
710   Journal of Seismology 2 (3): 257-265, https://doi.org/10.1023/a:1009723017040, 1998.

Morell, K. D., Styron, R., Stirling, M., Griffin, J., Archuleta, R., and Onur, T.: Seismic hazard analyses from geologic and geomorphic data: Current and future challenges, Tectonics, 39, e2018TC005365, https://doi.org/10.1029/2018TC005365, 2020.

Moulin, A., Benedetti, L., Rizza, M., Jamšek Rupnik, P., Gosar, A., Bourlès, D., Keddadouche, K., Aumaître, G., Arnold, M.,
715   Guillou, V., and Ritz, J.-F.: The Dinaric fault system: large-scale structure, rates of slip, and Plio-Pleistocene evolution of the transpressive northeastern boundary of the Adria microplate, Tectonics, 35 (10), 2258–2292, doi:10.1002/2016TC004188, 2016.

Najafabadi, A. J., Haberland, C., Le Breton, E., Handy, M. R., Verwater, V. F., Heit, B., Weber, M., and the AlpArray and AlpArray SWATH-D Working Groups: Constraints on crustal structure in the vicinity of the Adriatic Indenter (European
720   Alps) from Vp and Vp/Vs local earthquake tomography, J. Geophys. Res.: Solid Earth, 127, e2021JB023160, https://doi.org/10.1029/2021JB023160, 2022.

Placer, L., Vrabec, M., and Celarc, B.: The bases for understanding of the NW Dinarides and Istria Peninsula tectonics, Geologija, 53 (1), 55–86, doi:10.5474/geologija.2010.005, 2010.

Pondrelli, S., Salimbeni, S., Ekström, G., Morelli, A., Gasperini, P., and Vannucci, G.: The Italian CMT dataset from 1977 to
725   the present, Phys. Earth Planet. Interiors, 159 (3-4), 286–303, doi:10.1016/j.pepi.2006.07.008, 2006.

Poli, M. E., and Zanferrari, A.: The seismogenic sources of the 1976 Friuli earthquakes: a new seismotectonic model for the Friuli area, Boll. Geofis. Teorica Ed. Appl., 59 (4), 463–480, doi:10.4430/bgta0209, 2018.

Poljak, M., Gosar, A., and Živčić, M.: Active tectonics in Slovenia, Geology of the Adriatic area, International Geological Congress on the Adriatic Area (ADRIA 2006), Urbino, 19-20 June 2006 (Bologna, Italy, University of Bologna, Department
730   of Earth and Geological-Environmental Sciences), 15–24, 2010.

Rajh, G.: Raziskave strukture Zemljine skorje v severozahodnih Dinaridih z metodo lokalne seizmične tomografije = Investigations of the Earth's crust structure in the Northwestern Dinarides using local earthquake tomography method, Doctoral dissertation,   University   of   Ljubljana,   Ljubljana,   Slovenia,   https://repozitorij.uni-lj.si/IzpisGradiva.php?lang=eng&id=143236, last access: 14 July 2023, 2022.

735   Rajh, G., Zupančič, P., Živčić, M., Gosar, A., and Čarman, M.: Analiza največjih magnitud in globin žarišč potresov v Sloveniji za namen ocenjevanja potresne nevarnosti, in Raziskave s področja geodezije in geofizike 2016: zbornik del, edited by: Kuhar, M., Čop, R., Gosar, A., Kobold, M., Kralj, P., Ličer, M., Skok, G., Stopar, B., Vreča, P., and Čarman, M., 39-49, Fakulteta za gradbeništvo in geodezijo, Ljubljana, Slovenia, 2017.

Rajh, G., and Gosar, A.: Uporaba orodij GIS v analizi magnitude in globine potresov v Sloveniji za potrebe ocenjevanja
740   potresne nevarnosti, in *Pokrajina v visoki ločljivosti*, GIS v Sloveniji, edited by: Ciglič, R., Geršič, M., Perko, D., and Zorn, M., 1: 9-25, Založba ZRC, Ljubljana, Slovenia, ISBN: 9789610501121, 2018.

Natural Hazards
and Earth System
Sciences
Discussions

Rajh, G., Stipčević, J., Živčić, M., Herak, M., Gosar, A., and the AlpArray Working Group: One-dimensional velocity structure modeling of the Earth's crust in the northwestern Dinarides, Solid Earth, 13, 177–203, https://doi.org/10.5194/se-13-177-2022, 2022.

745   Reiter, L.: Earthquake Hazard Analysis: Issues and Insights, Columbia University Press, New York, ZDA, 254 pp, 1990.

Schmid , S. M., Fügenschuh, B., Kounov, A., Mat¸enco, L., Nievergelt, P., Oberhänsli, R., Pleuger, J., Schefer, S., Schuster, R., Tomljenović, B., Ustaszewski, K., and van Hinsbergen, D. J. J.: Tectonic units of the Alpine collision zone between Eastern Alps and western Turkey, Gondwana Res. 78, 308–374, doi:10.1016/j.gr.2019.07.005, 2020.

Serpelloni, E., Vannucci, G., Anderlini, L., and Bennett, R. A.: Kinematics, seismotectonics and seismic potential of the eastern
750   sector of the European Alps from GPS and seismic deformation data, Tectonophysics, 688, 157–181, doi:10.1016/j.tecto.2016.09.026, 2016.

Shedlock, K. M., Giardini, D., Grünthal, G. and Zhang, P.: The GSHAP Global Seismic Hazard Map, Seismol. Res.Lett., 71(6), 679-686, 2000.

Stipčević, J., Herak, M., Molinari, I., Dasović, I., Tkalčić, H., and Gosar, A.: Crustal Thickness Beneath the Dinarides and
755   Surrounding Areas from Receiver Functions, *Tectonics,* 39 (3), https://doi.org/10.1029/2019tc005872, 2020.

Stipčević, J., Tkalčić, H., Herak, M., Markušić, S., and Herak, D.: Crustal and uppermost mantle structure beneath the External Dinarides, Croatia, determined from teleseismic receiver functions, *Geophys. J. Int.,* 185 (3), 1103-1119, https://doi.org/10.1111/j.1365-246X.2011.05004.x, 2011.

Šket Motnikar, B., Zupančič, P., Živčić, M., Atanackov, J., Jamšek Rupnik, P., Čarman, M., Danciu, L., and Gosar, A.: The
760   2021 seismic hazard model for Slovenia (SHMS21): overview and results, B. Earthq. Eng., 20, 1-30, 10.1007/s10518-022-01399-8, 2022.

Vrabec, M., and Fodor, L.: Late Cenozoic tectonics of Slovenia: structural styles at the Northeastern corner of the Adriatic microplate, in: The Adria microplate: GNSS geodesy, tectonics and hazards (NATO science series IV, Earth and environmental Sciences 61), edited by: Pinter, N., Grenerczy, N., Weber, J., Stein, S., and Medak, D., Dordrecht, Netherlands, Springer, 151–
765   168, 2006.

Ward, S. N.: On the consistency of earthquake moment release and space geodetic strain rates: Europe, Geophys. J., 135 (3), 1011-1018, 10.1046/j.1365-246X.1998.t01-2-00658.x, 1998.

Weber, J., Vrabec, M., Pavlovčič-Prešeren, P., Dixon, T., Jiang, Y., and Stopar, B.: GPS-derived motion of the Adriatic microplate from Istria Peninsula and Po Plain sites, and geodynamic implications, Tectonophysics, 483, 214–222,
770   doi:10.1016/j.tecto.2009.09.001, 2010.

Youngs, R. R., and Coppersmith, K. J.: Implications of Fault Slip Rates and Earthquake Recurrence Models to Probabilistic Seismic Hazard Estimates, B. Seismol. Soc. Am., 75, 939 – 964, 1985.

ZAMG: Austrian Bulletin of Regional and Teleseismic events recorded with ZAMG-Stations in Austria, Geosphere, Austria, https://www.zamg.ac.at/cms/de/geophysik/erdbeben/erdbebenarchiv last access: 15 June 2023, 1998-2014.

775   ZAMG: Austrian Earthquake Catalogue (Computer file), Central Institute of Meteorology and Geodynamics, Vienna, Austria, 2002.

Zupančič, P., Cecić, I., Gosar, A., Placer, L., Poljak, M., and Živčić, M.: The earthquake of 12 April 1998 in the Krn Mountains (Upper Soča valley, Slovenia) and its seismotectonic characteristics, Geologija, 44 (1), 169–192, https://doi.org/10.5474/geologija.2001.012, 2001.